



Unraveling the Mesozoic and Cenozoic Tectonothermal Evolution of the Eastern Basque-Cantabrian Zone–Western Pyrenees by Low-Temperature Thermochronology

I. Defelipe, D. Pedreira, J. Pulgar, P. Beek, M. Bernet, R. Pik

► To cite this version:

I. Defelipe, D. Pedreira, J. Pulgar, P. Beek, M. Bernet, et al.. Unraveling the Mesozoic and Cenozoic Tectonothermal Evolution of the Eastern Basque-Cantabrian Zone–Western Pyrenees by Low-Temperature Thermochronology. *Tectonics*, 2019, 38 (9), pp.3436-3461. 10.1029/2019TC005532 . hal-02394183

HAL Id: hal-02394183

<https://hal.univ-lorraine.fr/hal-02394183>

Submitted on 10 Nov 2021

HAL is a multi-disciplinary open access archive for the deposit and dissemination of scientific research documents, whether they are published or not. The documents may come from teaching and research institutions in France or abroad, or from public or private research centers.

L'archive ouverte pluridisciplinaire **HAL**, est destinée au dépôt et à la diffusion de documents scientifiques de niveau recherche, publiés ou non, émanant des établissements d'enseignement et de recherche français ou étrangers, des laboratoires publics ou privés.



Distributed under a Creative Commons Attribution 4.0 International License

Tectonics

RESEARCH ARTICLE

10.1029/2019TC005532

Key Points:

- The Cinco Villas massif was buried beneath several kilometers of Mesozoic sediments and was exhumed in the early-middle Eocene by a S vergent fault
- The Oroz-Betelu massif was buried below the Pamplona basin before experiencing a rapid exhumation in the Bartonian-Priabonian
- The Leiza extensional detachment (eastern Basque-Cantabrian basin) was reactivated as a thrust system in the early Eocene

Correspondence to:

I. DeFelipe,
irene.defelipe@gmail.com

Citation:

DeFelipe, I., Pedreira, D., Pulgar, J. A., van der Beek, P. A., Bernet, M., & Pik, R. (2019). Unraveling the Mesozoic and Cenozoic tectonothermal evolution of the eastern Basque-Cantabrian zone–western Pyrenees by low-temperature thermochronology. *Tectonics*, 38, 3436–3461. <https://doi.org/10.1029/2019TC005532>





Received 18 FEB 2019

Accepted 21 AUG 2019

Accepted article online 24 AUG 2019

Published online 24 SEP 2019

Unraveling the Mesozoic and Cenozoic Tectonothermal Evolution of the Eastern Basque-Cantabrian Zone–Western Pyrenees by Low-Temperature Thermochronology

I. DeFelipe^{1,2} , D. Pedreira¹ , J. A. Pulgar¹, P. A. van der Beek³ , M. Bernet³ , and R. Pik⁴

¹Departamento de Geología, Universidad de Oviedo, Oviedo, Spain, ²Now at Institute of Earth Sciences Jaume Almera, ICTJA-CSIC, Barcelona, Spain, ³Institut des Sciences de la Terre, Université Grenoble Alpes, Grenoble, France, ⁴Centre de Recherches Pétrographiques et Géochimiques, CNRS-Université de Lorraine, Nancy, France

Abstract Low-temperature thermochronology studies have increased our knowledge of the orogenic processes along the Pyrenean-Cantabrian mountain belt by placing time constraints on the exhumation history of its rocks. However, a significant gap in the data existed between the western Pyrenees and the central Cantabrian Mountains, hampering a comprehensive view of the tectonothermal evolution along the belt. We present a new apatite fission track and zircon (U-Th)/He (ZHe) data set for the eastern Basque-Cantabrian zone–western Pyrenees. Apatite fission track central ages cluster in the Eocene-Oligocene. ZHe samples can be separated into two groups: Group 1 depicts clustered ZHe ages-eU concentration (Cinco Villas massif) and Group 2 depicts dispersed ZHe ages-eU concentration (Alduides massif and a Paleozoic rock pinned along the Leiza thrust). A sample from the Oroz-Betelu massif shows intermediate behavior. Inverse modeling suggests that samples from Group 1 reached 240–280 °C in the Late Cretaceous, implying deep sedimentary burial of the Cinco Villas massif before its major exhumation phase, most probably in the early to middle Eocene, postdating the phase of rapid exhumation of the western part of the Leiza thrust. The sample from the Oroz-Betelu massif, far from the Mesozoic exhumed mantle domain, experienced maximum temperatures close to 200 °C by burial beneath the Jaca-Pamplona basin. It was later exhumed in the hanging wall of the Gavarnie thrust in the Bartonian-Priabonian. This work provides new insights into the tectonothermal evolution of the Basque massifs and the inversion of a hyperextended margin.

1. Introduction

The Pyrenean-Cantabrian mountain belt extends along the northern border of the Iberian Peninsula for ~1,000 km in an east-west direction (Figure 1a). This belt formed as a result of the convergence between the Eurasian plate and the Iberian subplate from Late Cretaceous to Miocene times (e.g., Choukroune & ECORS Team, 1989; Muñoz, 1992; Rosenbaum et al., 2002; Teixell et al., 2018; Vergés et al., 1995). Throughout most of the Mesozoic, this area was affected by lithospheric extension, related to opening of the North Atlantic Ocean. This episode gave rise to the Bay of Biscay and to deep basins in the Pyrenean realm (e.g., García-Mondéjar et al., 1996; Jammes et al., 2009; Lagabrielle et al., 2010; Pedreira et al., 2015; Tugend et al., 2014, 2015; Ziegler, 1989). The northern border of the Iberian subplate was marked at that time by a spreading center from 8°W toward the west (present-day coordinates), an exhumed mantle domain from 8°W to ~4.2°W, and variably thinned continental crustal domains to the south and east, with very deep sedimentary basins and local mantle exhumation occurring along the Pyrenean realm (DeFelipe et al., 2017; Jammes et al., 2009; Lagabrielle et al., 2010; Lagabrielle & Bodinier, 2008; Roca et al., 2011; Ruiz et al., 2017; Tugend et al., 2014, 2015). Around the SE corner of the present-day Bay of Biscay, the Basque-Cantabrian basin developed as one of the most strongly subsiding basins of the Iberian periphery during the Aptian-Cenomanian (García-Mondéjar et al., 1996; Rat, 1988). Alpine convergence resulted in the inversion of these hyperextended crustal domains with intracontinental collision in the Pyrenees (Beaumont et al., 2000; Muñoz, 1992; Teixell et al., 2016, 2018), whereas shortening and uplift of the Mesozoic passive margin farther west created a coastal range: the Cantabrian Mountains (Alonso et al., 1996; Gallastegui et al., 2002; Pedreira et al., 2015; Pulgar et al., 1996; Quintana et al., 2015). Although along-strike differences in the orogenic style are evident, there is structural continuity between both mountain ranges (e.g., Pedreira

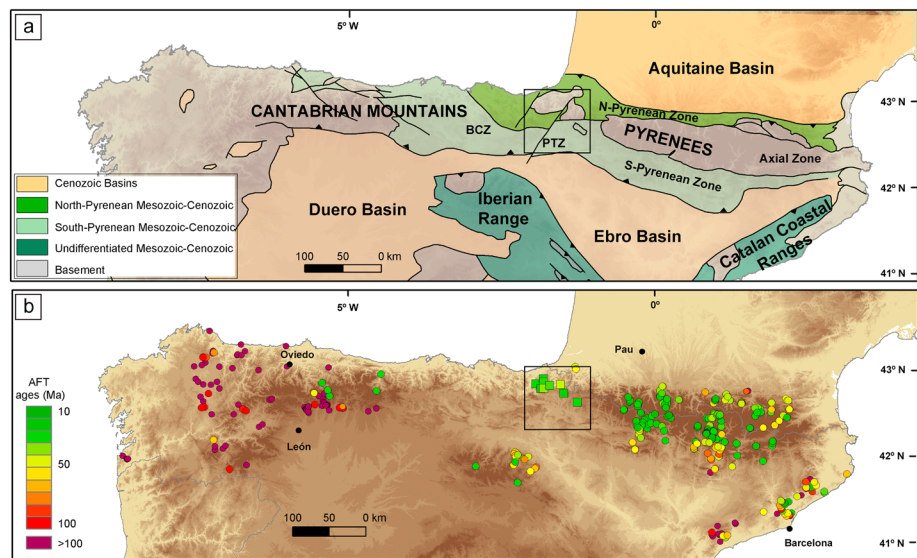


Figure 1. (a) Simplified geological map of northern Spain and southern France (BCZ: Basque-Cantabrian zone; PTZ: Pamplona Transfer Zone). The black square represents the study area (detailed geological map in Figure 2a). (b) Apatite fission track (AFT) data from northern Spain and southern France. Squares are the AFT ages obtained in this work and circles are AFT ages from the literature (Beamud et al., 2011; Bosch et al., 2016; Carrière, 2006; Del Rio et al., 2009; Fillon et al., 2013, 2016; Fillon & van der Beek, 2012; Fitzgerald et al., 1999; Gibson et al., 2007; Grobe et al., 2010, 2014; Jolivet et al., 2007; Juez-Larré & Andriessen, 2006; Labaume, Meresse, Jolivet, & Teixell, 2016; Labaume, Meresse, Jolivet, & Lahfid, 2016; Martín-González et al., 2012; Maurel et al., 2008; Metcalf et al., 2009; Morris et al., 1998; Mouthereau et al., 2014; Pérez-Arlucea et al., 2005; Rahl et al., 2011; Rat et al., 2019; Rushlow et al., 2013; Sinclair et al., 2005; Vacherat et al., 2014, 2016; Yelland, 1990).

et al., 2007). In this tectonic setting, the Basque-Cantabrian basin was also inverted and incorporated into the Pyrenean-Cantabrian mountain belt, forming the Basque-Cantabrian zone, which is characterized by a smoother topography with lower average elevation than the adjacent parts of the belt (Figure 1).

The unique characteristics of this orogen (wide range of pre-tectonic configurations from east to west, limited and variable along-strike amount of convergence, good geological and geophysical knowledge, good accessibility and outcrop conditions, etc.) make it an excellent target to study the spatial and temporal evolution of both lithospheric extension, tectonic inversion, and mountain building processes. For that reason, it has attracted the interest of numerous international research groups, with large geological/geophysical projects developed particularly during the last decade (Topo-Iberia, Topo-Europe PYRTEC, Pyramid, Pyrope, Orogen, and RGF-BRGM, among others). The Pyrenean-Cantabrian mountain belt is also a key region to place constraints on kinematic models for Iberia, a topic that has been strongly discussed recently (e.g., Barnett-Moore et al., 2017, 2016, 2018; Nirrengarten et al., 2018; van Hinsbergen et al., 2017). Discriminating between the different kinematic models requires good temporal constraints on the different phases of the tectonic evolution of the Pyrenean-Cantabrian-Bay of Biscay system. Low-temperature thermochronology provides valuable estimates of relatively shallow-rock cooling ages and rates, which can be related to rock exhumation due to extensional or contractional deformation.

The Cenozoic exhumation history of the Pyrenees s.s. is relatively well known due to the excellent Cenozoic syntectonic record and numerous thermochronological studies carried out mainly on the Variscan granites cropping out in the Axial Zone, and also on the foreland fold-and-thrust belts (e.g., Beamud et al., 2011; Bosch et al., 2016; Fillon et al., 2013; Fillon & van der Beek, 2012; Fitzgerald et al., 1999; Gibson et al., 2007; Jolivet et al., 2007; Labaume, Meresse, Jolivet, & Teixell, 2016; Labaume, Meresse, Jolivet, Teixell, & Lahfid, 2016; Mouthereau et al., 2014; Rahl et al., 2011; Rushlow et al., 2013; Sinclair et al., 2005). The combination of several thermochronometers and inverse modeling techniques revealed a complex exhumation history in this part of the belt, with greater and younger exhumation on the southern side and most rapid exhumation rates between the late Eocene and Oligocene (Beamud et al., 2011; Bosch et al., 2016; Fillon & van der Beek, 2012; Fitzgerald et al., 1999; Gibson et al., 2007; Labaume, Meresse, Jolivet, Teixell, &

Lahfid, 2016; Whitchurch et al., 2011). In the South Pyrenean Central Unit, Fillon et al. (2013) inferred syn-tectonic burial from the Late Cretaceous to the late Miocene, reaching temperatures of 70–95 °C. Toward the west, in the northern part of the Jaca basin, the base of the Tertiary sequence locally reached temperatures of up to ~240 °C, interpreted as due to a local thermal anomaly (Labaume, Meresse, Jolivet, Teixell, & Lahfid, 2016). A cooling event since the late Miocene has been assigned to re-exhumation of the southern flanks of the Pyrenees after burial during a phase of endorheism and basin overfilling (e.g., Coney et al., 1996; Fillon & van der Beek, 2012; Fitzgerald et al., 1999).

The exhumation history of the Cantabrian Mountains is less well constrained due to the scarcity of Cenozoic syntectonic sediments and to the difficulties in obtaining precise biostratigraphic control for those that are present. Low-temperature thermochronology studies in the Cantabrian Mountains have been mainly focused on the western part, where crystalline rocks of the Paleozoic basement are suitable for thermochronological analysis on apatite and zircon (Grobe et al., 2010, 2014; Martín-González et al., 2012). However, Alpine exhumation is limited in that part of the belt, and the thermochronological ages are generally pre-Cenozoic (Figure 1b). Only a few attempts have been made to sample the sedimentary rocks of the central part of the Cantabrian Mountains, where the relief and the amount of Cenozoic exhumation is greater (Carrière, 2006; Fillon et al., 2016). Fillon et al. (2016) inferred a substantial amount of Alpine exhumation (up to 8–10 km) between the late Eocene and the middle Oligocene (from 39 to 29 Ma) for the central Cantabrian Mountains.

As it can be readily observed in Figure 1b, an important gap of thermochronological information, specifically in apatite fission track (AFT) dating, exists in the Basque-Cantabrian zone and in the western Pyrenees. The main aim of this study is to reduce this gap, shedding light on the Alpine exhumation history of the Paleozoic massifs that crop out in that region (the Basque massifs) and to place it in the context of the Alpine evolution of the entire Pyrenean-Cantabrian mountain belt. In particular, we aim to date the main exhumation phases of the Basque massifs east and west of the Pamplona Transfer Zone (which marks the eastern border of the Basque-Cantabrian basin; Figure 1a), and to quantify the rate and amount of exhumation since the onset of convergence. In this work we use AFT and zircon (U-Th)/He (ZHe) analyses, including forward and inverse modeling of the data, to constrain thermal histories. These are well-established techniques for determining times and rates of cooling in the shallow crust that can be used to quantify rock denudation (Reiners & Brandon, 2006; Wagner, & van der Haute, 1992).

2. Geological Setting

The study area is located in the transition between the Pyrenees and the Cantabrian Mountains, specifically along the eastern border of the Basque-Cantabrian zone (Figures 1 and 2a). The NNE-SSW trending Pamplona Transfer Zone (PTZ; also named the Pamplona Fault, pale gray band in Figure 2a) has traditionally been considered as the boundary between the Pyrenees and the Cantabrian Mountains (e.g., DeFelipe et al., 2017; Larrasoana, Parés, Millán, et al., 2003; Pedreira et al., 2003, 2007; Vacherat et al., 2017). The PTZ represents a paleogeographic and structural boundary that played a major role during the Cretaceous extension. It marks the eastern lateral border of the deep Cretaceous Basque-Cantabrian basin (DeFelipe et al., 2018; García-Mondéjar et al., 1996; Rat, 1988), whereas to the east of the PTZ, the main Cretaceous depocenter is displaced toward the north, in the Arzacq-Mauléon basin (Larrasoana, Parés, Millán, et al., 2003; Masini et al., 2014; Vacherat et al., 2017). The PTZ also partitioned the Alpine compressional deformation: east of it, all major structures are south vergent, whereas west of it several north vergent thrusts are also present. The PTZ is not clearly visible at the surface, but it can be traced by an alignment of diapirs of Upper Triassic evaporites and shallow earthquake epicenters (Larrasoana, Parés, Millán, et al., 2003; Ruiz, Gallart, et al., 2006).

One of the most distinctive features in this area is the presence of basement outcrops forming the Basque massifs: Cinco Villas, Alduides, and Oroz-Betelu (Figure 2a). These massifs are composed of Ordovician to Permian rocks (Campos, 1979; Del Valle et al., 1973; Velasco et al., 1987) disconnected from the large outcrop of pre-Mesozoic rocks that forms the Pyrenean Axial Zone. The European or Iberian affinity of these Paleozoic units (whether they belonged to the northern or southern margin during the Mesozoic rifting event) has been widely discussed. Since the Iberian Peninsula rotated about 35° during the Cretaceous with respect to stable Europe (van der Voo, 1969), paleomagnetism has been one of the most widely used

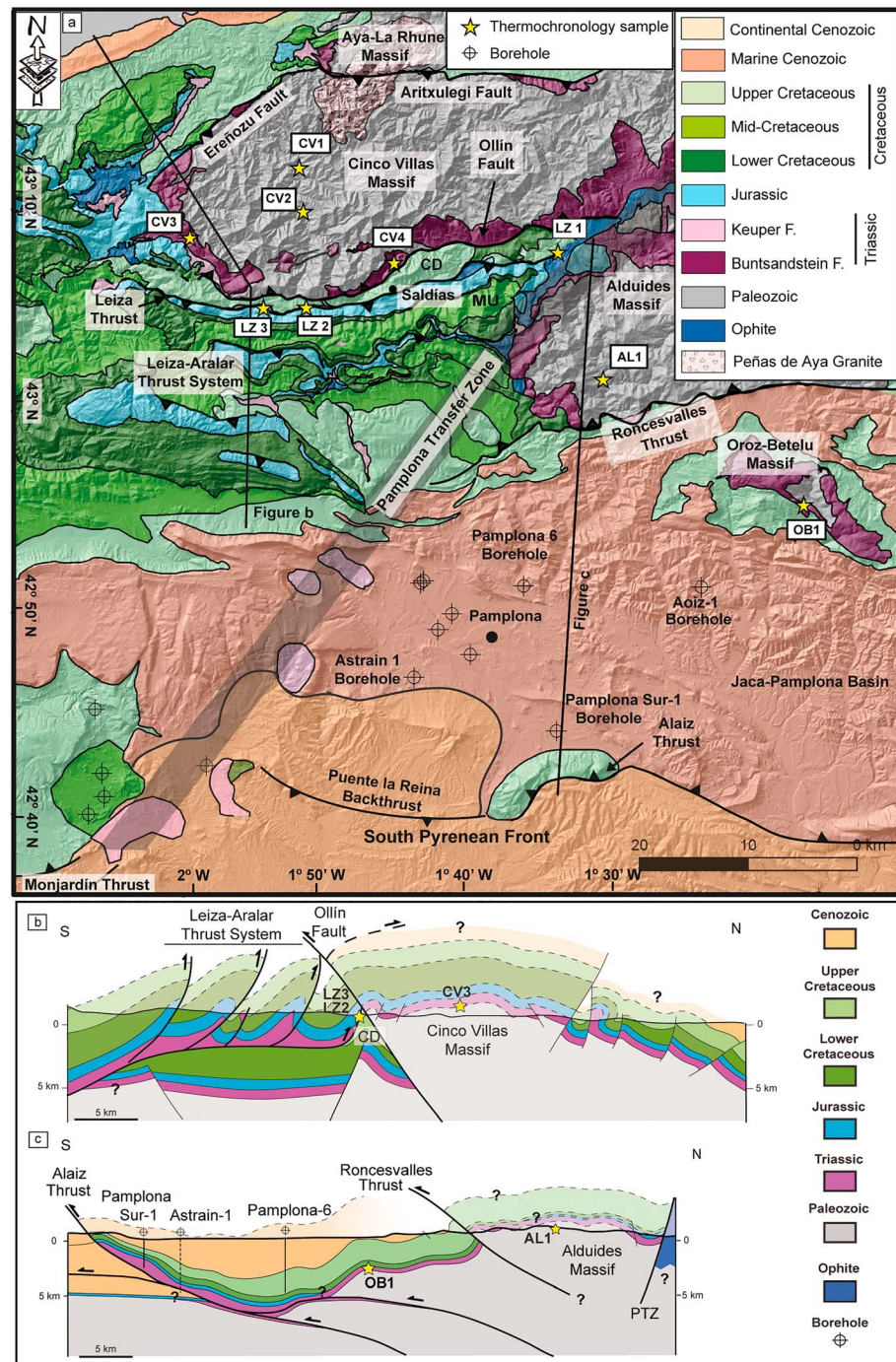


Figure 2. (a) Geological map of the study area with sample location. Black lines represent the cross sections of panels b and c. The pale gray band shows the location of the Pamplona Transfer Zone. See location in Figure 1a. The geological mapping was modified from Campos & García-Dueñas (1972); Carbayo et al. (1972, 1977); Del Valle (1974); Del Valle et al. (1972, 1973); Gabaldón et al. (1983, 1984); Knausse et al. (1972); Puigdefábregas et al. (1976); Ramírez Merino et al. (1984). Boreholes are taken from Lanaja (1987). CD: Central Depression; MU: Marble Unit. (b) Schematic geological cross section west of the Pamplona Transfer Zone, crossing the Cinco Villas massif and the Leiza-Aralar Thrust System (after DeFelipe et al., 2018). (c) Schematic geological cross section in the eastern side of the Pamplona Transfer Zone, from the Aldudes massif to the southern orogenic front. The Astrain-1 borehole, which cuts the Cenozoic beneath the frontal thrust, was projected orthogonally onto the section from a relatively long distance (see Figure 2a), and the basal depths for the Cenozoic and the Upper Cretaceous were modified to depict a more gradual change between the Pamplona Sur-1 and Pamplona-6 boreholes. Thermochronology samples were projected onto the section at the level of the corresponding lithology.

techniques for determining the affinity of the Paleozoic units. Early works showed that the Oroz-Betelu massif belonged to the Iberian side (van der Voo, 1969), and the Cinco Villas massif to the European side (van der Voo & Boessenkool, 1973). However, further research on the southern border of the Cinco Villas and Alduides massifs showed a complex pattern of rotations, the interpretation of which is not straightforward (Larrasoña, Parés, del Valle, & Millán, 2003; Oliva-Urcia et al., 2012; Schott & Peres, 1988). Larrasoña, Parés, del Valle, and Millán (2003) proposed a wide domain of distributed deformation at the “plate” boundary, formed by a set of fault-bounded blocks undergoing differential rotations in which the massifs behaved independently with respect to Eurasia and Iberia. Oliva-Urcia et al. (2012), using new and revisited data, emphasized the difficulty in determining the affinity of the Basque massifs by means of paleomagnetic data. Hence, other methods to discern the Iberian or European affinity are needed and will be discussed below.

The lowermost member of the Mesozoic cover, the Lower Triassic Buntsandstein-facies red sandstones (Campos, 1979; Diez et al., 2005), crop out at the borders of the Basque massifs and were extensively sampled for the paleomagnetic studies discussed above. Arostegui et al. (1987) also sampled these Lower Triassic sandstones and established affinity groups based on several compositional variables extracted from the X-ray diffraction of the <2- μ m fraction. They found two groups: one represented by the Cinco Villas massif samples, which they associated with the European plate, and the other represented by the Alduides and Oroz-Betelu massifs samples, which they associated with the Iberian subplate. Middle Triassic Muschelkalk-facies rocks hardly crop out in the study area, whereas the Upper Triassic Keuper-facies evaporites crop out in diapirs and along thrusts and anticlines. The Keuper-facies evaporites are locally intruded by Upper Triassic to Lower Jurassic subvolcanic basic rocks (known as “ophites”; González et al., 2007; Rossy et al., 2003). Jurassic rocks are mainly limestones and marls deposited in shallow-marine open platforms (Aurell et al., 2003; Bádenas, 1996) and crop out in several E-W bands south of the Cinco Villas massif and in local basins NW of this massif. Cretaceous rocks can be grouped in three units: (i) the Purbeck-Weald Complex (uppermost Jurassic-Barremian), formed by sandstones and limestones (Rat, 1988); (ii) the Urgonian complex (Aptian to early Cenomanian), formed by marls and limestones (Bodego et al., 2015; García-Mondéjar et al., 1996; Rat, 1988, and references therein); and (iii) Upper Cretaceous flysch sediments and platform deposits (limestones, marls and sandstones) (Brusset et al., 1997; Mathey et al., 1999; Rat, 1988; Tilhac et al., 2013). Cenozoic rocks crop out in a narrow band along the coast, in the South Pyrenean Zone, and in the Ebro foreland basin. Paleocene to lower Eocene rocks were deposited in marine environments, deeper in the northern outcrops (including flysch facies) than in the present South Pyrenean Zone (platform deposits; Rat, 1988). In the South Pyrenean synorogenic basin, the depocenter and the deformation front migrated southward from the Late Cretaceous to the early Miocene (e.g., Labaume, Meresse, Jolivet, & Teixell, 2016; Labaume & Teixell, 2018; Teixell, 1998). In this region and east of the PTZ, the platform deposits were overlapped by Eocene siliciclastic flysch sediments including carbonate megabreccias (Barnolas & Teixell, 1994; Labaume et al., 1985; Payros et al., 1999, 2007). This turbiditic basin is known here as the Pamplona basin, or Jaca-Pamplona basin in a wider regional context. The turbidites are covered by Bartonian to early Priabonian marls and upper Priabonian to Oligocene continental detrital sediments, the later cropping out extensively to the east and west of the study area. Upper Oligocene to Miocene continental deposits crop out in the southern part of the study area, corresponding to the northwestern border of the Ebro foreland basin.

There are several major structures in the area, including the Ollín Fault, the Leiza-Aralar Thrust System, the Roncesvalles Thrust, the South Pyrenean Front (represented by the Alaiz Thrust along the studied transect), and the PTZ (Figure 2a). The Ollín reverse fault runs along the southern border of the Cinco Villas massif and uplifted the massif over a narrow basin to the south, the *Dépression Intermédiaire* or Central Depression (Bodego et al., 2015; Iriarte, 2004; Lamare, 1936). Outcrops in the Central Depression mostly expose Upper Cretaceous rocks, showing evidence of Albian to Turonian hydrothermalism with maximum temperatures of 185 °C, as estimated by fluid inclusion microthermometry (Iriarte, 2004; Iriarte et al., 2011). The Leiza-Aralar Thrust System is located south of the Central Depression and is formed by up to five north vergent thrust sheets, each one carrying Upper Triassic to Lower Cretaceous rocks in its hanging wall (DeFelipe et al., 2018). The northern part of the Leiza-Aralar Thrust System, called *Nappe des Marbres* or Marble Unit (Lamare, 1936), shows evidence of high-temperature metamorphism. Maximum metamorphic temperatures are estimated at 500 to >550 °C, based on mineral assemblages and Raman spectroscopy analyses (Ducoux et al., 2018; Martínez-Torres, 2008), and are found close to the Leiza thrust (the northernmost

outcropping thrust of the Leiza-Aralar Thrust System). Toward the south, the metamorphic grade decreases progressively. In this context, the Leiza-Aralar Thrust System corresponds to the inversion of the extensional detachment system that led to an exhumed/unroofed mantle domain in the axis of the Cretaceous extensional system (DeFelipe et al., 2018). East of the PTZ, the exhumation domain is displaced toward the north, in the Mauléon basin (e.g., Jammes et al., 2009, 2014; Saspiturry et al., 2019). This is another argument to support that the Cinco Villas massif belonged to the European side of the rift, whereas Alduides and Oroz-Betelu massifs belonged to the Iberian side.

At the junction between the Leiza thrust and the PTZ, a mix of allochthonous blocks of peridotites, granulites, ophites, marbles, and Mesozoic (meta)sedimentary rocks embedded in a Keuper-facies clayey-evaporitic matrix crops out, forming a complex unit, the Ziga mélange (DeFelipe et al., 2017). East of the PTZ, the Roncesvalles Thrust places the Alduides massif on top of the Cenozoic sediments of the Jaca-Pamplona basin. The Alaiz Thrust is generally considered the southern frontal structure of the range in this sector, thrusting the Jaca-Pamplona basin over the Ebro foreland basin and bringing Upper Cretaceous rocks to the surface. However, deformation still progressed farther south, favored by the presence of upper Eocene-lower Oligocene evaporitic layers in the Ebro basin, giving rise to the Tafalla Thrust and some blind thrusts and detachment folds (Pueyo Anchuela, 2004). Between the Alaiz Thrust and the PTZ, the orogenic front is more complex, with the emergence of a backthrust known as the Puente la Reina Backthrust (Figure 2a). West of the PTZ, the local frontal structure is known as the Sierra de Cantabria or Monjardín thrust.

Figures 2b and 2c show two cross sections through the Cinco Villas and Alduides massifs (see locations in Figure 2a) west and east of the PTZ respectively. The most remarkable features are the difference in thickness of the Jurassic and Lower Cretaceous sedimentary rocks and the vergence of the structures. In the western section (Figure 2b) several Mesozoic normal faults were inverted to form the current Leiza-Aralar Thrust System. These thrusts are north vergent and root into a sole thrust in the Keuper-facies evaporites at the base of the basin (the former extensional detachment), leading to a thin-skinned tectonic style. Slices of Carboniferous and Triassic sandstones are brought up along the Leiza thrust, providing appropriate lithologies for thermochronological analysis. Immediately north of this fault, the band of Upper Cretaceous rocks that crop out in the Central Depression is very narrow at present, but the Mesozoic extent of this subbasin is assumed to have been larger. It has been partially overthrust at both margins, especially by the Leiza-Aralar Thrust System (DeFelipe et al., 2018), which puts into contact two areas with different Mesozoic tectonothermal histories. The Ollín Fault is defined by an alignment of seismic hypocenters that reaches 30-km depth (Ruiz, Gallart, et al., 2006) in a thick-skinned tectonic style. In the eastern section (Figure 2c) the main faults are south vergent and the PTZ shows a significant accumulation of ophites. To the south, the Roncesvalles Thrust superposes the Alduides massif over the Jaca-Pamplona basin. Within this basin, Upper Cretaceous sedimentary rocks thicken to the north, whereas the Jurassic and Lower Cretaceous rocks are significantly thinner than in the western cross section (Figure 2b). Another hidden transfer structure is probably present between this section and the outcrop of the Oroz-Betelu massif (Pueyo Anchuela et al., 2007), with the Mesozoic thinning farther to the east (note the absence of Jurassic and Lower Cretaceous on top of the Permian in the Oroz-Betelu massif). Along this section, we propose that the Jurassic observed in the Pamplona Sur-1 and Astrain-1 boreholes disappears toward the north, as it is absent in the hanging wall of the Roncesvalles Thrust, but we assume continuity of a thin layer of Lower Cretaceous. The Jaca-Pamplona basin is thrust toward the south by the Alaiz Thrust, which represents the major South Pyrenean frontal structure separating the fold-and-thrust belt from the Ebro foreland basin. Basement uplift beneath the northern half of the Jaca-Pamplona basin is interpreted to be due to the presence of two basement thrusts that can be considered as lateral equivalents to the Guarga and Gavarnie thrusts toward the east (e.g., Teixell et al., 2016; Teixell & García-Sansegundo, 1995).

3. Sampling Strategy and Methodology

Since granitic rocks in the study area are restricted to the relatively small Peñas de Aya granite in the Cinco Villas massif (Campos, 1979; Figure 2a), we extended our sampling to coarse-grained Paleozoic and Mesozoic sandstones across the area. Out of a total of 34 samples collected, only 9 yielded sufficient apatite grains for AFT dating and 4 of these showed sufficient horizontal confined tracks for length measurements.

Table 1
Sample Description and Geographic Location

Sample	Structural unit	Depositional age	Lithology	Latitude	Longitude	Altitude (m)
CV1	Cinco Villas M.	Up. Carboniferous	Sandstone	43.198	−1.861	713.00
CV2	Cinco Villas M.	Up. Carboniferous	Sandstone	43.163	−1.855	713.00
CV3	Cinco Villas M.	Triassic	Sandstone	43.143	−1.983	578.00
CV4	Cinco Villas M.	Triassic	Sandstone	43.12	−1.753	534.00
OB1	Oroz-Betelu M.	Triassic	Sandstone	42.908	−1.296	813.00
AL1	Alduides M.	Up. Carboniferous	Sandstone	43.021	−1.519	717.00
LZ1	Leiza thrust		Granulite	43.123	−1.569	280.00
LZ2	Leiza thrust	Up. Carboniferous	Sandstone	43.084	−1.853	673.00
LZ3	Leiza thrust	Triassic	Sandstone	43.086	−1.899	537.00

ZHe dating was carried out in 6 of the AFT-dated samples (see sample locations in Figure 2a). Samples are from Carboniferous and Triassic sandstones from the Basque massifs, two tectonic slices along the Leiza thrust and a mafic granulite (sample LZ1) from the Ziga mélange (DeFelipe et al., 2017; Table 1).

Apatite and zircon crystals were separated from crushed rocks by heavy liquid and magnetic separation techniques following the procedure described by Kohn et al. (2018). Apatite grains were mounted in epoxy resin and etched with 5.5 M HNO₃ for 20 s at ~21 °C at the ISTERRE fission track laboratory (*Université Grenoble Alpes*) in order to reveal spontaneous tracks. The external detector method was used for the AFT age estimations, attaching a low-U content sheet of mica to the surface of the mounts. Samples were irradiated in the FRM II Research Reactor (*Technische Universität München*) together with the Durango and Fish Canyon Tuff age standards. Induced tracks were revealed by etching the mica sheet with HF (48% reagent grade) for 18 min at 20 °C, and ages were determined by the ζ calibration method. Fission track grain-age data were analyzed with the BinomFit program (Brandon, 2005).

For ZHe dating, careful selection of zircon grains from the heavy fraction (>3.3 g/cm³) of the samples was performed under a 120X binocular microscope to avoid any visible mineral or fluid inclusions and to allow determination of grain size (length and width). Bipyramidal single grains were packed individually in Pt containers and loaded into an ultra-high vacuum sample holder sealed with a synthetic sapphire viewport. Aliquots were outgassed at 1500 °C for 35 min, using a Diode Laser System combined with a pyrometer. Grains were subsequently analyzed for He concentrations with a VG603 noble gas mass spectrometer (Godard et al., 2009; Pik et al., 2003). A second outgassing was performed on each aliquot to check that He extraction was complete (<5 % remaining). After complete He extraction, Pt packets were retrieved for U, Th, and Sm following the procedure developed by Tibari et al. (2016). The precision of ZHe ages determined with this procedure is about 6%. ZHe ages were corrected for α -ejection according to the procedure of Ketcham et al. (2011). The full data set of AFT and ZHe dating is available in DeFelipe et al. (2019).

In order to constrain the time-temperature (t - T) history, forward and inverse modeling of thermochronological ages and track length distributions were performed with two programs: HeFTy (Ketcham, 2005) and QTQt (Gallagher, 2012). These thermochronological modeling programs use different approaches, each one with its strengths and weaknesses (see discussions in Flowers et al., 2015, 2016; Gallagher, 2016; Gallagher & Ketcham, 2018; Vermeesch & Tian, 2014, 2018). For forward modeling we used the HeFTy code and the zircon radiation-damage annealing model of Guenther et al. (2013). Inverse models were obtained with the QTQt program, which employs a Bayesian approach to test a large number of possible t - T paths across the model space (in our case, 100,000 paths). For each thermal history, the method solves the data-specific predictive model and data fit (likelihood) function. In this modeling we included the AFT and ZHe ages as input data. Track length measurements were used for samples LZ2 and CV2, which had sufficient available track lengths. Barbarand et al. (2003) suggested that for complex thermal histories, a minimum of 100 track lengths may be representative, but depending on the sample, mean track lengths stabilizes between 50 and 120 tracks. In our inverse modeling, we used the annealing model of Ketcham et al. (2007) for AFT and the radiation damage model of Guenther et al. (2013) for ZHe.

Exhumation rates were calculated based on the t - T paths predicted by QTQt for the Eocene. Already in the Eocene, the thermal anomaly that prevailed in the Cretaceous had decayed and the heat flow was equivalent to that of the present day (64 mW/m²) as suggested by thermal modeling in the Basque-Cantabrian zone by

Table 2
Detrital Apatite Fission Track Ages (External Detector Method)

Sample	n	ρ_s (10^5 cm^{-2})	N_s	ρ_i (10^5 cm^{-2})	N_i	P (χ^2)(%)	Dispersion(%)	Central age (Ma)	± 2 σ	U (ppm)	± 2 σ	N (TL)	MTL (μm)	± 2 σ	MDpar (μm)	± 2 σ
CV1	27	5.94	370	17.4	1083	51.7	5.1	28.9	2	36	2				1.69	0.29
CV2	43	6.86	715	17.3	1802	5.4	15.5	34.3	2.1	36	2	49	13	1.45	1.6	0.28
CV3	30	7.42	390	20.4	1071	16.9	17.1	31.8	2.5	42	3				1.7	0.36
CV4	28	10.8	526	23.5	1142	0	31.8	41.5	3.6	49	3	34	12.90	1.24	1.65	0.14
AL1	18	5.55	135	11.2	273	1.9	37.5	51.4	8	24	3				—	
OB1	22	6.71	387	15	864	0.2	27.9	38.2	3.7	31	2	30	13.1	2	1.7	0.32
LZ 1	29	1.21	174	2.62	377	98.9	0.2	40.1	3.9	5	1				—	
LZ 2	30	7.14	583	16.8	1368	48.4	5.4	36.1	2.2	35	2	70	12.85	1.64	1.6	0.18
LZ 3	22	7.09	228	18.2	584	0	42.3	39.9	5	38	3				1.69	0.35

Note. n : number of dated grains; ρ_s and ρ_i : density of spontaneous and induced tracks; N_s and N_i : number of spontaneous and induced tracks; $P(\chi^2)$: probability of a mixed-age population; N (TL): number of measured track lengths; MTL: mean track length (c axis projected); and MDpar: mean Dpar values.

Gómez et al. (2002). In this approach, we calculated exhumation rates during the Eocene, dividing the predicted t - T paths in linear segments assuming geothermal gradients of 20 and 25 °C/km, and a surface temperature of 10 °C and using the weighted mean temperature predicted by QTQt. The assumed values for the geothermal gradient are consistent with the regional geothermal gradients determined by Labaume, Meresse, Jolivet, Teixell, and Lahfid (2016) for the Rupelian in the western part of the Jaca basin, using vitrinite reflectance measurements and Raman spectroscopy. These authors suggested values between 23 and 26 °C/km for that age, consistent with the present-day mean gradient of 22.6 °C/km in the detached South Pyrenean Unit (Fernández et al., 1998). Temperature offset between samples in subvertical profiles in the western Axial Zone and Chaînons Béarnais also point to mean geothermal gradients of 25 °C/km, with no major variation throughout the Paleogene (Bosch et al., 2016). Finally, these are also the range of geothermal gradient values used by Fillon et al. (2016) in their thermochronologic study of the central Cantabrian Mountains, allowing a direct comparison of results between both zones.

4. Thermochronological Ages

Table 2 and Figure 3 show the AFT ages obtained. The fission track age of each sample is expressed as the central age (Galbraith & Laslett, 1993) with $\pm 2\sigma$ uncertainties. Central ages have geological significance in terms of cooling ages of the samples (Labaume, Meresse, Jolivet, Teixell, & Lahfid, 2016) if samples were buried to reach temperatures higher than the Partial Annealing Zone (PAZ), being completely reset, and if they subsequently cooled rapidly through the PAZ. However, in a sample that contains apatite crystals with strongly variable annealing properties, age dispersion will increase in relation to the residence time in the PAZ during postannealing cooling. If samples were buried to temperatures corresponding to the PAZ, they will be partially reset. The single-grain ages are dispersed due to the diversity of the cooling ages in the source area and/or to variability in annealing rates of individual grains. In this case, the central age is without geological significance, mixing source-area cooling ages and the age at which the sediment exited the PAZ in the inverted basin.

Radial plots (Galbraith, 1990; Figure 3) depict the deconvolution of single-grain ages into a set of component distributions (Brandon, 2002). Samples CV1, CV2, CV3, LZ1, and LZ2 contain a single age population whereas two-age populations were detected in the rest of the samples using the statistical approach of IsoplotR (Vermeesch, 2018). Samples including two-age populations may have been partly reset for the AFT system or may reflect variable annealing or inclusions in their apatites.

Samples from the Cinco Villas massif and its Triassic cover (to simplify the descriptions, we will consider hereafter the Buntsandstein-facies rocks as part of the massifs) show central ages or young peak age in case of a mixed-age population (sample CV4) between 34.4 ± 2 and 28.9 ± 2 Ma. The two samples from the Aldudes and Oroz-Betelu massifs have young peak ages of 27.2 ± 5.2 and 31.7 ± 3.3 Ma, respectively.

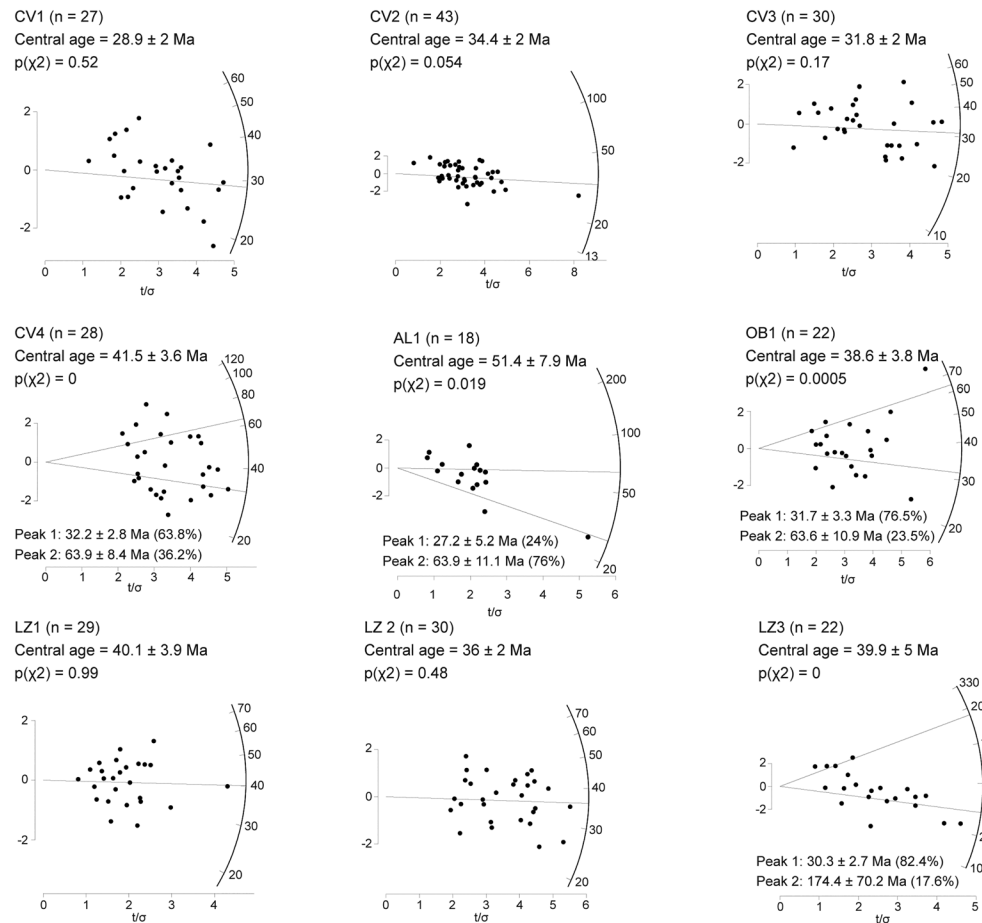


Figure 3. Radial plots (Galbraith, 1990) for each sample obtained with IsoplotR (Vermeesch, 2018); n is the number of apatite grains counted and t/σ represents the relative precision for each single-grain age. Samples CV4, AL1, OB1, and LZ3 show a mixed-age population, which can be deconvolved into two peak ages.

These two, together with sample CV4, show a secondary peak age at 63–64 Ma. Sample LZ3, on the other hand, shows a secondary peak of Mesozoic age (174.4 ± 70.2 Ma) represented by 17.6% of the grains. Sample LZ1, a basic granulite from the Ziga mélange (DeFelipe et al., 2017), shows the oldest single-age population of the whole data set (40.1 ± 3.9 Ma).

Two samples from the Cinco Villas massif (CV2 and CV4), the sample from the Oroz-Betelu massif, and a Carboniferous sandstone slice along the Leiza thrust (LZ2) provided track length data, with mean lengths ranging from 12.85 to 13.1 μm . Dpar measurements performed on selected samples show mean values ranging between 1.6 and 1.7 μm . Apatite grains with relatively low Dpar values (≤ 1.75 μm) can generally be considered fast-annealing, near-end-member calcic-fluorapatites. This is the dominant apatite variety in most crustal rocks (Carlson et al., 1999; Donelick et al., 2005).

Table 3 and Figure 4 show the ZHe ages. Samples can be separated into two groups according to their ZHe ages and effective uranium content ($eU = U + 0.235 \times \text{Th}$, ppm). Group 1 comprises samples with low dispersion of ZHe ages and eU concentrations, all of them from the Cinco Villas massif (CV1, CV2, and CV3). ZHe ages in this group range between 46.9 ± 2.8 and 29.6 ± 1.8 Ma, and eU contents are concentrated between 241 and 732 ppm. Group 2 comprises more dispersed ZHe ages and/or eU concentrations, observed in samples AL1 (Alduides massif) and LZ2 (Leiza thrust). Sample OB1 from the Oroz-Betelu massif shows slightly dispersed ZHe ages and eU contents, but not as much as samples belonging to Group 2, thus representing an intermediate behavior. Generally, thermochronologic ages of partially reset detrital zircon grains present several types of ZHe age-eU correlations caused by variations in predepositional (inherited) age, radiation-damage-induced He diffusion kinetics, and grain size among other factors. Furthermore, each

Table 3
Zircon (U-Th)/He Ages

Sample	Length (μm)	Width (μm)	FT	eU (ppm)	⁴ He (nmol/g)	Th (ppm)	U (ppm)	Sm (ppm)	ZHe age (Ma)	Corrected ZHe age (Ma)	Standard deviation
CV1	327	120	0.87	272	43.4	72	255	5	29.6	34.0	2.0
	324	122	0.87	689	96.2	279	623	7	25.9	29.6	1.8
	306	131	0.87	250	39.4	64	234	4	29.3	33.5	2.0
	253	156	0.87	496	97.4	36	487	3	36.5	42.0	2.5
	237	102	0.85	529	89.6	95	507	2	31.5	37.1	2.2
	265	140	0.88	256	37.5	39	247	5	27.2	31	1.9
CV2	263	111	0.85	337	51.4	48	326	6	28.3	33.3	2.0
	322	123	0.87	471	71.2	135	440	3	28.0	32.1	1.9
	262	105	0.85	363	55.4	149	328	11	28.3	33.2	2.0
	291	115	0.86	467	77.7	211	418	7	30.8	35.7	2.1
CV3	195	61	0.78	258	51	55	245	11	36.6	46.9	2.8
	184	76	0.8	241	31.7	67	226	17	24.4	30.4	1.8
	149	69	0.77	732	115	319	657	53	29.2	37.8	2.3
LZ2	297	123	0.87	148	71.2	49	136	5	89.4	102.8	6.2
	233	141	0.86	134	52.5	31	127	3	72.5	84.2	5.1
	209	125	0.84	1,260	221.2	64	1,245	9	32.6	38.8	2.3
	234	107	0.84	1,812	260.7	358	1,727	7	26.7	31.7	1.9
OB1	201	141	0.86	90	16.5	50	78	5	34.1	39.8	2.4
	208	109	0.84	318	62.3	116	291	5	36.3	43.1	2.6
	207	108	0.84	168	29.4	70	151	15	32.6	38.7	2.3
	226	126	0.86	190	28.1	153	155	13	27.4	31.9	1.9
	272	74	0.83	807	86.6	198	760	2	19.9	24.1	1.4
	230	102	0.85	572	111.7	131	541	5	36.2	42.8	2.6
AL1	225	108	0.85	457	140.1	151	422	14	56.9	67	4
	206	106	0.83	292	229.3	85	272	5	145.9	175.1	10.5
	245	93	0.83	323	155.6	41	313	2	89.4	107.6	6.5
	240	142	0.87	121	28.5	85	101	5	43.8	50.4	3.0
	209	86	0.82	1,471	78	93	1,449	7	9.8	11.9	0.7

Note. eU: effective uranium content ($U + 0.235 \times Th$); FT: correction factor.

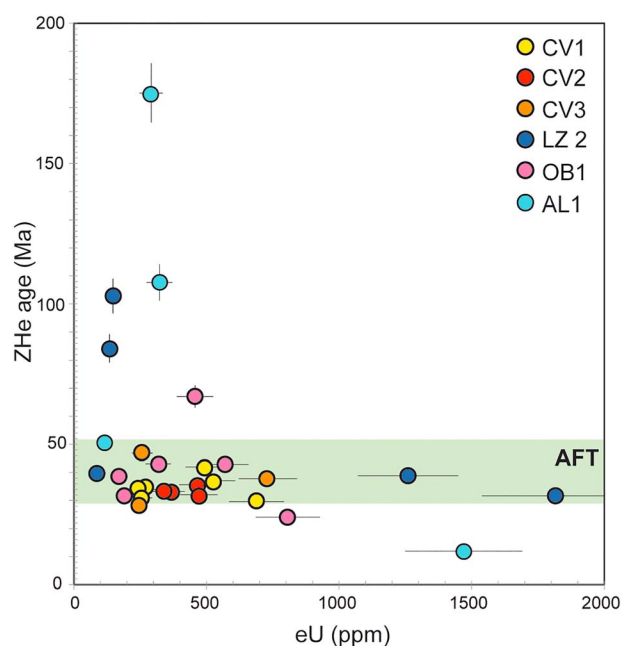


Figure 4. ZHe age (Ma) versus eU (ppm) for each zircon crystal analyzed. The green field represents the apatite fission track (AFT) central age range obtained for the whole data set.

zircon grain will possess a specific amount of inherited radiation damage and He concentration. As a consequence, ZHe ages may not fall along a single ZHe age-eU curve, producing either positive, negative or both correlations between ZHe age and eU concentrations (Guenther et al., 2015).

5. Modeling of the Thermochronological Data

5.1. Forward Modeling

We first performed forward modeling of the ZHe ages of samples interpreted to be partially reset (OB1 and samples belonging to Group 2; Figure 5). This approach aims to test the plausible range of thermal scenarios that can reproduce an observed data set of ZHe ages and eU concentrations. These results also provide a sense of the range of ZHe age-eU correlation produced by different t - T paths and demonstrate the match (or lack thereof) between observations and models for specific paths. Positive correlations can be expected if α -damage accumulation is relatively low and the sample cools slowly through the Partial Retention Zone (PRZ), so that damage in-growth and diffusion happen simultaneously. Conversely, if damage accumulation is relatively high (because of a long predepositional history and relatively low temperatures), then a thermal pulse results in a negative correlation, or significant He loss may occur at low temperatures. Grains with different amounts of radiation

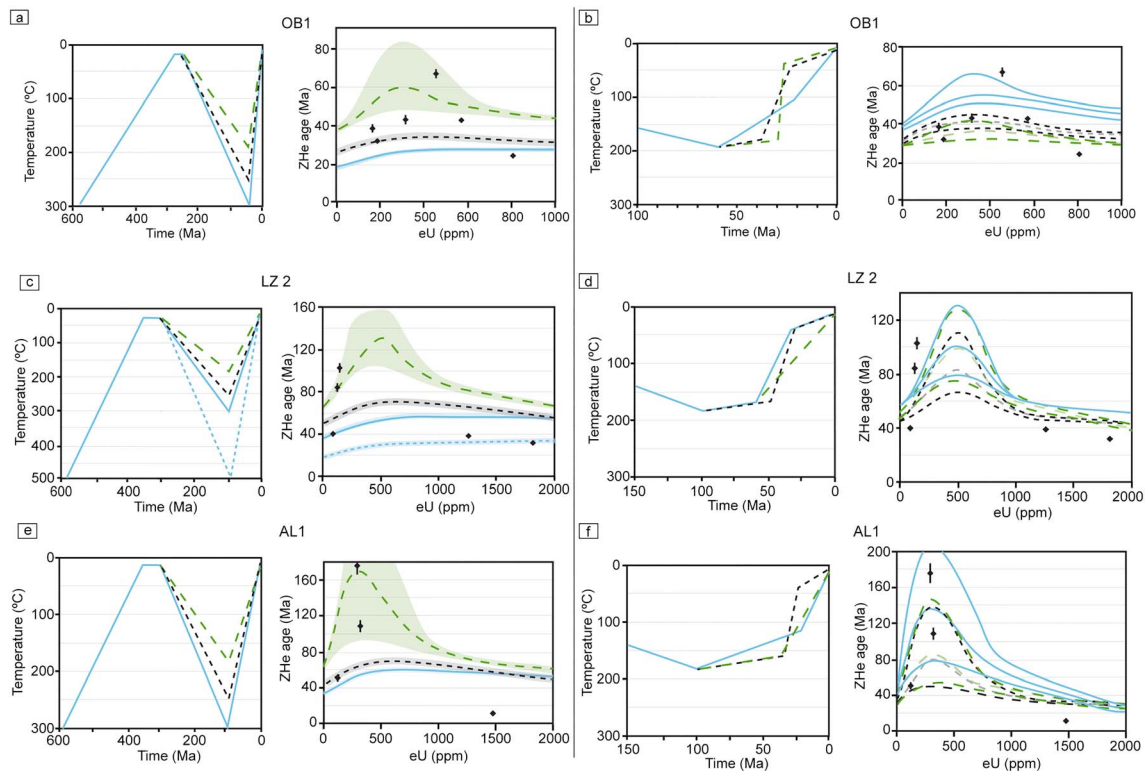


Figure 5. Forward models for samples OB1 (a, b), LZ2 (c, d), and AL1 (e, f) using HeFTy (Ketcham, 2005). Left panels in each figure show t - T paths from 600 Ma. For visual purposes, panels b, d, and f depict the t - T histories from 100 Ma for OB1 and 150 Ma for LZ2 and AL1, although they have been run with the same pre-deposition thermal histories than in panels a, c, and e. Right panels show corresponding ZHe age-eU model output (lines and envelopes) and observed ZHe corrected ages data (black diamonds; standard deviation represented by vertical black lines). Lines in right panels represent the results for the mean grain size and envelopes represent the range of results according to the 2- σ grain size variation. Only the borders of the envelopes are represented as thin lines in panels b, d and f, to avoid color overlapping. (a, c, and e) forward models testing the maximum temperatures achieved during the mid-Cretaceous: 500 °C for sample LZ2 (dotted pale blue line); 300 °C (pale blue line); and 180–200 °C (broken green line). (b, d, and f) Forward models testing three different stepwise Cenozoic cooling trends.

damage, as well as an initial span of predepositional ages, are reset to varying degrees during a reheating event (Guenther et al., 2013).

We evaluated the ZHe age-eU correlations for different t - T histories. Left panels in Figure 5 represent the proposed t - T histories and right panels show the modeled ZHe age-eU curve for each history. The possible t - T paths are based on the following geological constraints: (i) peak temperature was achieved in the mid-Cretaceous for samples located near the hyperextended domain (LZ2 and AL1) or Paleogene for OB1, located farther from the hyperextended domain and buried by the Eocene Jaca-Pamplona basin; (ii) samples were at surface conditions at their depositional age in the Carboniferous (LZ2 and AL1) and the Triassic (OB1); and (iii) samples were cooled initially from 570–580 Ma (U/Pb peak age in the Pyrenees; Mouthereau et al., 2014; Whitchurch et al., 2011) to their depositional age. We appended the predepositional t - T history to each of our model inputs to test the potential effect of inheritance in the ZHe ages (Guenther et al., 2015). In a first step (Figures 5a, 5c, and 5e) we tested three t - T histories to evaluate the maximum temperatures attained before the Alpine exhumation. These t - T paths reach temperatures comprised between 180 and 300 °C. Additionally, for LZ2, we tested the influence of the metamorphism with a maximum temperature of 500 °C. In a second step (Figures 5b, 5d, and 5f) we ran three different t - T histories for each sample to test the style of Cenozoic cooling. For visual purposes, these figures only depict the t - T history from 100 and 150 Ma (Figures 5b, 5d, and 5f), although they have been run following the predepositional history described above and depicted in Figures 5a, 5c, and 5e.

Figures 5a and 5b show the forward models for sample OB1. In the first step (Figure 5a), the scenarios that reach temperatures of 250 and 300 °C depict a slightly positive, almost flat ZHe age-eU correlation. The

scenario where maximum temperature reached 190 °C allows for a partial reset system, depicting both positive and negative correlation. Figure 5b tests the adjustment of the ZHe ages and eU for different Cenozoic cooling histories from a maximum temperature of 190 °C. Two of the scenarios proposed test a main cooling event during the Eocene-Oligocene, with different cooling rates. Predicted ZHe ages for these two paths range between 28 and 45 Ma, with a reasonably fit of the observed ages (except the oldest one). The third path explores a relatively constant cooling during the Paleogene, which predicts older ZHe ages.

Figures 5c and 5d show the forward models for sample LZ2. Four scenarios were tested in the first step, reaching maximum temperatures in the mid-Cretaceous of 500 °C (dotted pale blue line), 300 °C (pale blue line), 250 °C (broken black line), and 180 °C (broken green line). The three first scenarios depict a positive ZHe age-eU correlation followed by a flat or slightly negative correlation that does not fit the data. The scenario reaching a Cretaceous temperature of 180 °C predicted ZHe ages ranging from 64 to 160 Ma at 500 ppm and decreasing to 64 Ma at 2000 ppm. This scenario best accounts for partial resetting of the zircons. However, as the range of ZHe ages is not accurately adjusted, further modeling is shown in Figure 5d, where a maximum temperature of 180 °C is followed by stepwise Cenozoic cooling. The three scenarios proposed in this modeling predict overlapping ZHe ages-eU envelopes, with older ZHe ages predicted for 500 ppm and decreasing rapidly with increasing eU content. These results suggest that maximum temperatures registered during the Cretaceous in this sample may not have reached 500 °C; in that case zircons would have been completely reset leading to a positive, almost flat, ZHe age-eU curve. Thus, maximum Cretaceous temperatures of 180 °C and stepwise Cenozoic cooling are required to explain the partial reset ZHe system observed in LZ2.

Figure 5e displays the forward models for sample AL1 with a Cretaceous thermal event that reached 300 °C (pale blue line), 250 °C (broken black line), and 180 °C (broken green line). The two first scenarios show a slightly positive correlation followed by an almost flat ZHe age-eU relation. The third scenario predicts a positive to negative correlation covering a wide range of ZHe ages, thus accounting for a partial reset of the ZHe system. In order to further adjust the observed ZHe age-eU contents, we tested a stepwise Cenozoic cooling after a Cretaceous peak temperature of 180 °C. Figure 5f shows three scenarios for different Cenozoic cooling paths; they predict largely overlapping ZHe age-eU distributions, with oldest ages predicted for ~300 ppm and decreasing rapidly to less than 40 Ma for negligible eU contents or contents higher than ~1,000 ppm. In order to gain further insight into the range of possible t - T paths, we used an inverse modeling approach that will be described in the next section.

5.2. Inverse Modeling

In order to further test the maximum temperatures achieved before the Alpine exhumation, the age and rate of the Cenozoic cooling and the inheritance in the samples that are partially reset for the ZHe system, we performed inverse modeling of samples CV1, CV2, CV3, OB1, LZ2, and AL1. Modeling was done with the QTQt software (Gallagher, 2012) to retrieve the t - T paths from the input data. The input parameters were the individual AFT ages, the ZHe single-grain ages, the mean Dpar values, and the track length distributions when available. The output of the method is a collection of paths that are represented in a color scale indicating the probability of the thermal history curve passing through a particular temperature-time region (the posterior marginal distribution of temperature). It also provides the “best data fitting model” (maximum likelihood) and the “expected model” (the weighted mean from the posterior distribution). The difference between the observed and predicted ages is shown together with the predicted t - T paths in Figure 6. For the AFT age, QTQt represents the adjustment of the central age for every sample, independent of whether the sample shows a single or mixed-age population. A track length histogram is displayed for samples LZ2 and CV2. The only thermal constraint imposed for the inversions is the near-surface temperature at a short time interval centered in the depositional age; thus, the t - T paths are allowed to cover the full time-temperature space outside this interval.

Inverse modeling for sample CV1 (Figure 6a) predicts ages that differ from the observed data by less than 2 Ma for the AFT age or for the ZHe ages of 33.5 and 34 Ma. For the rest of the ZHe ages, maximum differences with the observed ages are 6 Ma. Sample CV2 has 49 measured track lengths; hence, we show inversions both with and without the track length measurements. The t - T path that was predicted without considering the track lengths (Figure 6b, upper panel) reproduces the AFT and ZHe ages well, with maximum age differences of less than 5 Ma. The results are consistent with those of CV1, suggesting rather

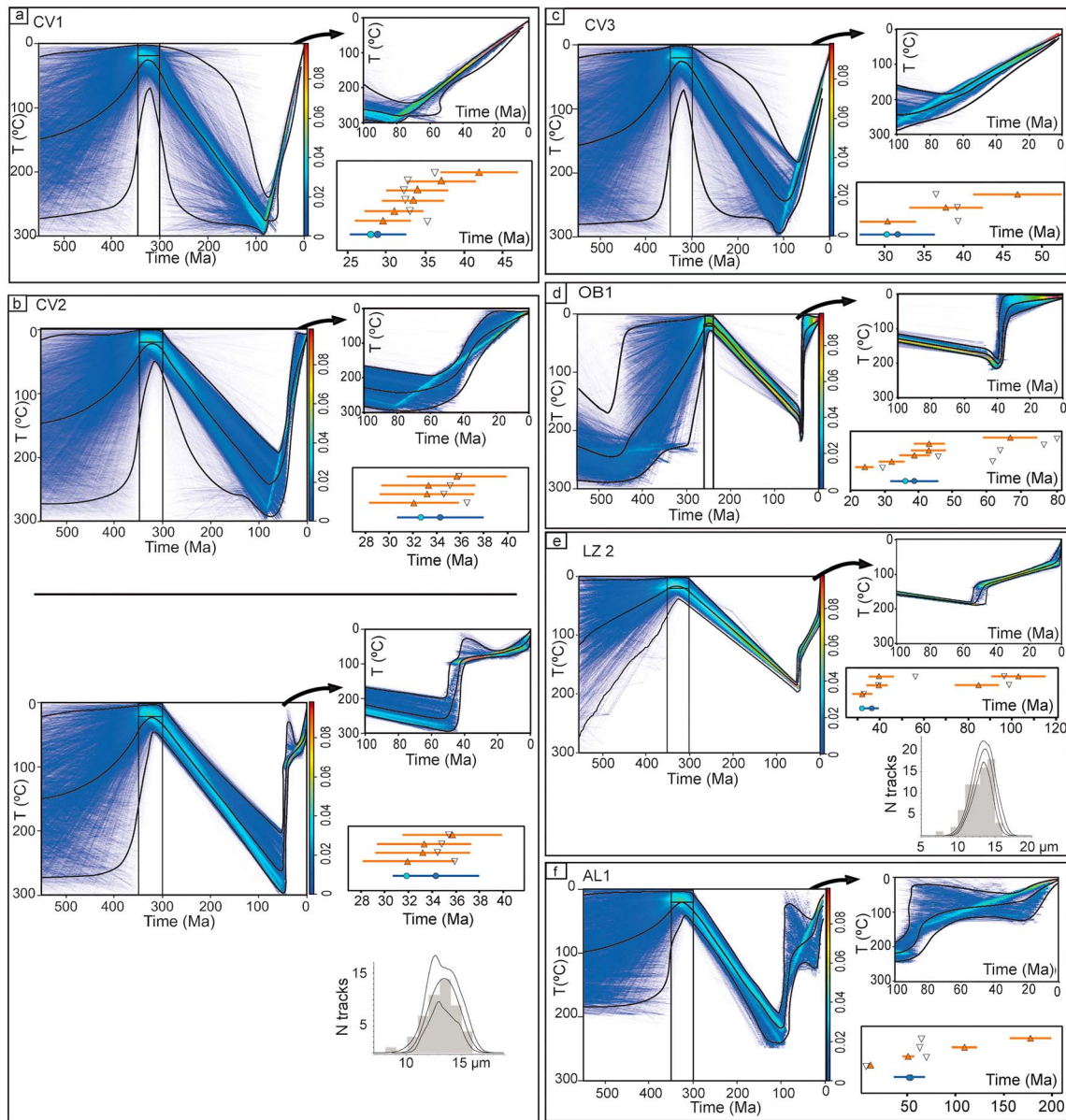


Figure 6. Inverse modeling for samples CV1 (a), CV2 (without– above– and with– below– track lengths; b), CV3 (c), OB1 (d), LZ2 (e), and AL1 (f) using QTQt (Gallagher, 2012) for 100,000 paths tried. Each figure is made up of three plots: (i) the t - T paths obtained including a predepositional inheritance and colored according to their probability (blue to red scale on the right-hand side of each model) with black curves representing the expected model (weighted mean model) and its 95% confidence interval and black squares the restrictions imposed; (ii) the t - T path in (i) expanded for the last 100 Ma; and (iii) the observed ZHe and AFT ages (dark blue circle and orange triangle respectively) and predicted ZHe and AFT ages according to the expected model (light blue circle and inverted white triangles respectively, with error bars marking the 2σ range). The observed track length distribution is displayed for sample LZ2 and CV2 with the mean track length distribution and its 95% confidence bounds in black lines (c -axis projected). AFT: apatite fission track.

monotonic cooling since the Late Cretaceous from maximum temperatures of 240–280 °C (weighted mean models). However, this simple cooling path may be a consequence of being underconstrained due to the missing track length information. We therefore tested an additional model including a fit to the track length distribution (Figure 6b, lower panel). In that case, the model predicts similar maximum temperatures (slightly higher for the weighted mean model) but reached in the Paleocene, the exhumation occurring at a much faster rate in the early to middle Eocene. The fitting of ZHe is very similar to the model without track lengths, but the AFT age is less well adjusted (although still within the error bounds). The implications of these different results will be discussed in the next section. The

modeling for sample CV3 suggests also a monotonic cooling since the mid-Cretaceous (Figure 6c). Predicted ages differ by less than 2 Ma from the observed AFT age and from the ZHe age of 37.8 Ma. However, the predicted ZHe ages show much less scatter than the observed ages.

The inverse modeling output for sample OB1 shows heating from the depositional age to 40 Ma, reaching a maximum temperature of 200 °C, then fast cooling to less than 40 °C from ~40 to 30 Ma, and final slow cooling (Figure 6d). The predicted AFT age for this sample differs from the observed age by 3 Ma, but the predicted ZHe ages are generally older than the observed ZHe ages.

The model for sample LZ2 (Figure 6e) is constrained by the AFT and ZHe ages and the track length distribution. In spite of being collected in the basal thrust of the Marble Unit, QTQt did not predict any *t-T* path reaching more than 190 °C, as imposed by the dispersion of measured ZHe ages. The weighted mean model output shows that these maximum temperatures were achieved during the early Eocene, with fast cooling between circa 55 and 45 Ma, followed by a slow cooling until 10 Ma and a final faster cooling. The observed and predicted AFT age differ by 4 Ma. The ZHe ages of 31 and 38.8 Ma differs from the predicted ages by less than 1 Ma, but the rest of the ZHe ages depart from the observed ages between 7 and 16 Ma.

Figure 6f shows the modeling results for sample AL1. The weighted mean model predicts a maximum temperature of ~220 °C at 100 Ma and Cenozoic cooling with a thermal stability period until the Miocene. The predicted AFT age and the ZHe age of 11 Ma differ from the observed ages by less than 8 Ma. Unfortunately, the rest of the predicted ZHe ages are concentrated between 62 and 68 Ma, whereas the observed ages show a significantly larger scatter.

6. Discussion

6.1. Interpretation of the Thermochronological Ages

AFT central ages are mostly Eocene and early Oligocene, although samples CV4, AL1, and OB1 (Figure 3) show an older age peak in the early Paleocene. In contrast, sample LZ3 shows an older peak in the Jurassic. The fact that the single-grain ages are much younger than the Paleozoic and Triassic stratigraphic ages argue for a totally reset AFT system. The strong dispersion of the single-grain ages specially highlighted in LZ3 could be explained by inclusions within the crystals that lead to errors in age determinations, as suggested for previous low-*T* thermochronological dating in the western Axial Zone (Bosch et al., 2016), or differences in the chemistry of individual grains.

In the Cinco Villas massif samples, CV1, CV2, and CV3, both the AFT and the ZHe ages record cooling related to the Alpine orogeny. Furthermore, the complete reset of the ZHe and AFT system implies relatively fast and continuous cooling through the PRZ and PAZ of both thermochronometers during the Alpine exhumation, also evidenced by the inverse modeling. Additionally, inverse modeling including track length measurements for sample CV2 predicts a stepwise Cenozoic thermal history with fast cooling through the ZHe-PRZ followed by a period of slow cooling since the late Eocene. These results point out that *t-T* paths through the PAZ may be underconstrained due to lack of track length measurements.

Sample LZ1 displays an AFT age of 40 Ma, indicating cooling during the middle Eocene fast enough through the PAZ to completely reset its apatites. This sample was collected from a granulite block embedded in the Ziga evaporitic mélange extruded during the inversion of the Leiza detachment system and cropping out in the junction of the Leiza thrust with the PTZ (DeFelipe et al., 2017).

The dispersion observed in the ZHe ages of samples from Group 2 (LZ2 and AL1) is due to a partially reset ZHe system, also possibly influenced by the grain size (Figures 5d and 5f), U and Th zonation, and zircon radiation damage (Guenther et al., 2013; Reiners, 2005). Inverse modeling (Figure 6) shows that totally reset samples (those belonging to Group 1) achieved a higher temperature (presumably by deeper burial) before its Cenozoic exhumation than those belonging to Group 2. Sample OB1 appears to show intermediate behavior between samples from Groups 1 and 2, but inverse modeling suggests that this sample reached the highest temperatures in the middle Eocene and did not exceed 200 °C (weighted mean model, Figure 6d). The results obtained for this sample point to a strongly but not totally reset ZHe system by burial under Mesozoic and pre-middle Eocene sediments.

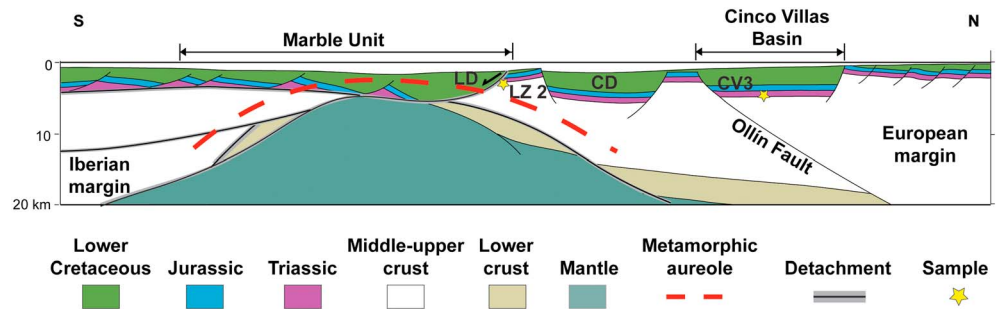


Figure 7. Tectonic reconstruction of the cross section of Figure 2b to the mid-Cretaceous with the probable location of samples LZ2 and CV3 (see DeFelipe et al., 2018, for details of the tectonic reconstruction). Tentative extension of the metamorphic aureole is indicated by the red dashed line. CD: Central Depression; LD: Leiza detachment system.

Regarding the inverse modeling for samples OB1, LZ2, and specially AL1 (those that are partially reset for the ZHe system), the predicted ZHe ages differ significantly from the observed ages and the ZHe age-eU dispersion cannot be adequately predicted by the QTQt software (Figures 6d–6f). Toward the east of the study area, in the western Axial Zone, inverse modeling carried out by Bosch et al. (2016) also found the same problem, being unable to predict a significant dispersion of the observed ZHe ages. These authors suggested that the differences between the observed and predicted ZHe ages could be due to a complex internal zonation in the zircon grains, which is not incorporated in the modeling. In spite of these limitations, the maximum temperatures achieved by samples OB1, LZ2, and AL1 before the Alpine exhumation seem to be relatively well constrained as the inversion results are essentially coherent with the requirements of the forward models to fit the first-order trends of the ZHe-eU plots.

6.2. Thermal Evolution During the Cretaceous Hyperextension

Some of the ZHe thermochronometric data provide pre-Cenozoic ZHe ages, thus registering a thermal inheritance prior to the Alpine orogeny. The high geothermal gradient (Gómez et al., 2002), metamorphism, hydrothermalism, and hot fluid circulation in the eastern Basque-Cantabrian basin during the Cretaceous (DeFelipe et al., 2017) led to a complex thermal history of the samples located in the Cretaceous rift margin. Figure 7 shows a reconstruction of the cross section of Figure 2b to the mid-Cretaceous (see DeFelipe et al., 2018 for further details on the crustal-scale tectonic reconstruction). At this stage, Cretaceous extension led to the formation of a hyperextended domain with local mantle unroofing in the easternmost Basque-Cantabrian basin. The Leiza detachment system put into contact mantle rocks in its footwall with Mesozoic sediments in its hanging wall, thus promoting metamorphism on the overlying sediments (DeFelipe et al., 2017). The sedimentary cover of this hyperextended domain was formed by a sequence of subbasins separated by south dipping normal faults in the hanging wall of the Leiza detachment system. During this extensional stage, Triassic Keuper-facies diapirs could have been formed as diapirism is described in other areas of the Basque-Cantabrian zone at that time (e.g., Bodego et al., 2018; Poprawski et al., 2016). These extensional faults were inverted during the Alpine orogeny, leading to the Leiza-Aralar Thrust System. During the tectonic inversion, the northernmost of these subbasins is interpreted to be totally eroded (DeFelipe et al., 2018) and Lower Triassic and Paleozoic rocks were wrenched and incorporated as tectonic slices along the Leiza thrust. Samples LZ2 and LZ3 belong to two of these tectonic slices. The lateral extension of the metamorphic aureole is constrained based on the outcrops of metamorphic rocks. However, a certain degree of uncertainty exists due to the Cenozoic erosion of part of the basin located on top of the exhumed/unroofed mantle domain and to the decrease of the metamorphic grade toward the west within the Marble Unit, where samples LZ2 and LZ3 are located. In fact, the maximum metamorphic temperatures of $>550^{\circ}\text{C}$ are estimated only toward the east of Saldías (Figure 2a; Ducoux et al., 2018; Martínez-Torres, 2008). At least in this eastern part of the Leiza detachment system, lower crust and mantle rocks were also wrenched and incorporated into the evaporitic/tectonic mélange of the sole thrust (DeFelipe et al., 2017) and were later extruded during tectonic inversion in the intersection with the PTZ (sample LZ1).

We projected the probable location of samples LZ2 and CV3 on the reconstruction of Figure 7. In the case of sample LZ2, its precise location during the Cretaceous is uncertain due to its unknown position beneath

the Mesozoic cover. However, since the ZHe ages are not totally reset, this sample should have reached $<190^{\circ}\text{C}$. In fact, in the adjacent Central Depression, hydrothermalism is estimated at maximum temperatures of 185°C (Iriarte et al., 2011). Thus, during the Cretaceous, sample LZ2 would most probably be located in the Paleozoic basement of the European margin, in the footwall of the Leiza detachment system, and far enough from the metamorphic aureole. Samples CV1, CV2, and CV3 were located even farther away from the metamorphic aureole, in the Paleozoic and Triassic rocks of the Cinco Villas massif. However, our inverse modeling results for these samples (Figures 6a, 6b, and 6c) show higher maximum temperatures ($240\text{--}280^{\circ}\text{C}$ for the expected weighted mean model) achieved at different times depending on whether we incorporate the available track lengths in the modeling (Paleocene) or not (mid-Cretaceous). Since this part of the t - T path is not constrained by the track length data, we consider the mid-Cretaceous age for the thermal maximum more reliable for three reasons: (i) it matches the regional thermal maximum anomaly responsible for the metamorphism of the Marble Unit and the alkaline magmatism of the Biscay Synclinorium (e.g., Castañares et al., 2001); (ii) the Paleocene geothermal gradient was already very close to the present-day gradient (Gómez et al., 2002), implying an unrealistic amount of sedimentary burial to reach those high temperatures; and (iii) an important remagnetization event affecting the Triassic Buntsandstein-facies materials of the Cinco Villas massif was also found to occur in the mid-Cretaceous (Larrasoña, Parés, del Valle, & Millán, 2003).

The Cinco Villas massif has been previously interpreted as a paleohigh for the Late Cretaceous (Mathey et al., 1999; Rat, 1988). Vacherat et al. (2017) also proposed for most of the Late Cretaceous a continental domain at the northeastern part of the Cinco Villas massif, supplying the Basque-Cantabrian basin with sediments. Although the Cretaceous lies unconformably on top of the Paleozoic in certain areas (e.g., Bodego et al., 2015), we stress here that this actually occurs in the Aya-La Rhune massif. This massif is located to the north of a prominent north directed thrust formed by the Ereñozu fault and its eastern continuation, the Aritxulegi (or Arichulegui) fault (Ábalos, 2016; Campos et al., 1975) (Figure 2a). We therefore suggest that this inverse fault may represent the inversion of a south dipping Mesozoic normal fault, allowing for a thicker sediment accumulation in the southern block. Our results point to a sufficient burial depth, at least for the western part of the Cinco Villas massif, to completely reset the ZHe system, reaching maximum temperatures in the mid-Cretaceous, probably under a rather high geothermal gradient. Hence, in the reconstruction of Figure 7, a relatively thick basin is proposed for the western border of the Cinco Villas massif, whereas toward the east, the Cretaceous sedimentary cover may have been reduced. Samples CV1 and CV2, representing Paleozoic rocks of the west and central part of the Cinco Villas massif, experienced a similar thermal evolution to CV3 (Triassic). However, as CV1 and CV2 had an eroded Paleozoic cover over them, to explain the same maximum temperatures before exhumation, thinning of the Cretaceous sediments toward the east is needed.

East of the PTZ, sample AL1 reached the maximum temperature during the mid-Cretaceous (Figures 5e, 5f, and 6f) although the inverse modeling for this sample does not provide a precise thermal history. Nevertheless, it is remarkable that mid-Cretaceous remagnetizations were also described in the Triassic rocks of this massif (Larrasoña, Parés, del Valle, & Millán, 2003). This area was probably close enough to the PTZ to experience a high geothermal gradient at that time.

Farther east, however, the Oroz-Betelu massif (sample OB1) was located far away from the hyperextended domain, and mid-Cretaceous remagnetizations were not observed in the Triassic cover of this massif (Larrasoña, Parés, del Valle, & Millán, 2003). Our modeling for this sample predicts the highest temperatures in the middle Eocene, when it reached its maximum burial depth below the synorogenic sediments of the Jaca-Pamplona basin, before the deformation front progressed south and exhumed this part of the belt.

6.3. Thermal Evolution During the Alpine Orogeny

After the extensional period in the Basque-Cantabrian zone, the Alpine orogeny yielded to basin inversion, mountain building, and exhumation of basement rocks. Figure 8 shows the best constrained thermal histories for the studied samples since the Late Cretaceous to the present with the main tectonic events at a regional scale indicated. Colored lines represent the expected t - T paths (weighted mean models) predicted by QTQt (Figure 6) and shaded green and orange bands represent the AFT PAZ and ZHe PRZ according to Reiners and Brandon (2006) for a hold time between 1 and 5 Ma (upper and lower boundaries indicating 90% and 10% retention respectively). Although differences between the thermal histories of each sample

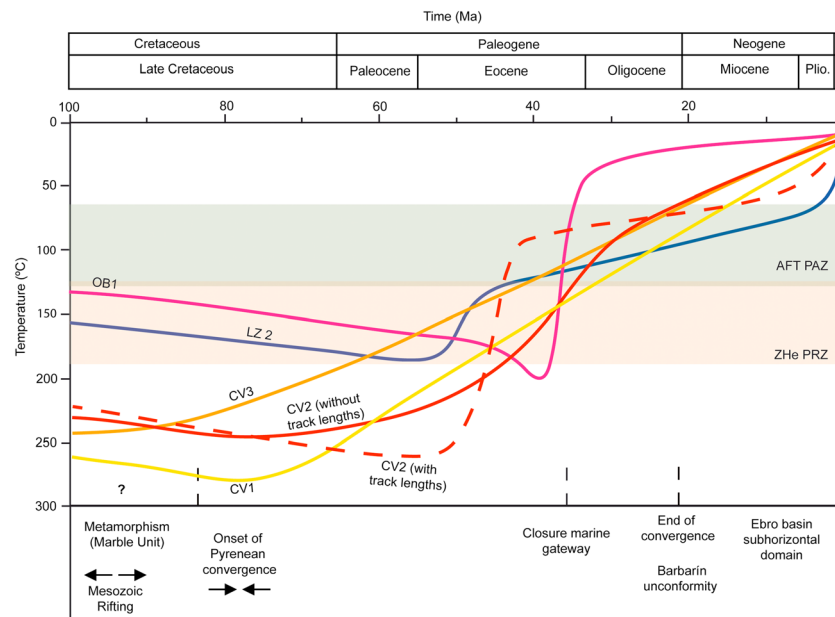


Figure 8. Schematic t - T history for the best constrained samples from the western Pyrenees and eastern Basque-Cantabrian zone with the main geological events depicted. The AFT Partial Annealing Zone (AFT PAZ) and ZHe Partial Retention Zone (ZHe PRZ) are indicated in shaded green and orange bands, respectively. The expected t - T paths correspond to the weighted mean models predicted by QTQt (Figure 6). AFT: apatite fission track.

exist, the general thermal history shows that the main Alpine cooling phase took place in the Eocene to early Oligocene.

Our inverse modeling suggests that samples belonging to the Cinco Villas massif (CV1, CV2 without track lengths, and CV3) experienced rather monotonic cooling since the Late Cretaceous (100–80 Ma). This result does not mean that the uplift related to the Pyrenean orogeny commenced at that time. As heat flow was decreasing after the end of crustal thinning, the thermal effect of increasing burial depth by postrift subsidence may cause a net cooling of the rocks (e.g., Ceriani et al., 2006). Hence, if the tectonic uplift is not rapid enough, it may be difficult to determine its onset from the shape of the cooling path. Track length data, however, may provide additional constraints, even if we must interpret them with caution due to their low number. They suggest a cooling path that we consider more geologically meaningful, with a sharper tectonically driven exhumation phase in the early to middle Eocene (Figure 8). This timing coincides with the onset of rapid exhumation in the western Pyrenees, where erosional unroofing in the hanging wall of the Lakora basement thrust yielded fast cooling at circa 50 Ma (Bosch et al., 2016; Hart et al., 2017; Teixell, 1998).

Sample LZ2, located during the Cretaceous in the footwall of the Leiza detachment system (Figure 7) was exhumed as a tectonic slice in the Leiza thrust since the early Eocene. Inverse modeling results show that the end of the period of higher exhumation rate for LZ2 predates the end of the period of higher exhumation rate for the Cinco Villas massif (Figure 8). These results may suggest that the Leiza detachment system was one of the earliest structures to accommodate the contractional deformation and that it was later overthrust by the Ollín Fault, superposing the Cinco Villas massif and its sedimentary cover over the Central Depression and the Marble Unit (Figure 2b; DeFelipe et al., 2018). This sequence of structures can also explain the steepening and local overturning of the thrust planes in the Leiza-Aralar Thrust System, in the footwall of the Ollín Fault (Martínez-Torres, 2008).

Finally, sample OB1 in the Oroz-Betelu massif was continuously buried below the thick sedimentary column of the Jaca-Pamplona basin, with a long residence time in the ZHe PRZ until the middle-late Eocene (Bartonian-Priabonian). This moment coincides with the overfilling of marine sediments in this basin and the transition to continental deposition (Barnolas & Gil-Peña, 2001; Costa et al., 2010), marking the onset of exposure and cooling by tectonic uplift and surface denudation. According to our modeling results, the

Table 4*Eocene Exhumation Rates and Burial Estimates for Samples CV1, CV2 (Without and With Track Lengths), CV3, OB1, and LZ2*

Sample	CV1	CV2 (without track lengths)	CV2 (with track lengths)	CV3	OB1	LZ2
Period (Ma)	55–34	55–34	50–40	55–34	40–34	55–45
Exhumation rate (km/Myr)	0.16 ± 0.02	0.24 ± 0.03	0.77 ± 0.08	0.13 ± 0.02	1.12 ± 0.12	0.25 ± 0.03
Burial (km)	7.8–9.8	8.6–10.8	10–12.5	6.4–8	7.6–9.5	7–9

Note. Values have been estimated based on the weighted mean temperatures predicted by QTQt (Figure 6) assuming a geothermal gradient ranging between 20 and 25 °C/km and a surface temperature of 10 °C.

exhumation of the Oroz-Betelu massif was rapid up to the early Oligocene. Ruiz, Gaspà, et al. (2006) considered that the anticline cored by the Paleozoic massif is related to a basement thrust, cut by the Aoiz-1 borehole (Figure 2a), in which Triassic rocks are found below the Paleozoic at 4.2 km depth. According to these authors, this basement thrust corresponds to the western prolongation of the Gavarnie thrust, cropping out farther east (e.g., Labaume & Teixell, 2018; Teixell, 1998; Teixell et al., 2016). In fact, the age of rapid cooling obtained for sample OB1 matches precisely the age of the Gavarnie thrust determined by dating of syntectonic sediments ahead of related structures south of the Oroz-Betelu massif (between the upper Lutetian and the Rupelian; García-Sansegundo & Barnolas, 2000) or in the Jaca-Pamplona basin (Priabonian-Rupelian; Labaume, Meresse, Jolivet, Teixell, & Lahfid, 2016; Teixell, 1996). It is also remarkably coincident with recent $^{40}\text{Ar}/^{39}\text{Ar}$ dating of synkinematic muscovites from a secondary thrust plane related to the Gavarnie thrust, which gave an age of 36.9 ± 0.2 Ma (Priabonian; Abd Elmola et al., 2018). In the cross section of Figure 2c, we have tentatively drawn a basement thrust that would be laterally equivalent to the Gavarnie thrust, although differences in depth and thickness of the sedimentary cover maybe due to the presence of lateral structures, as mentioned in section 2. We also included another basement thrust to the south that would be laterally equivalent to the Guarga thrust, the activity of which has been dated as Oligocene to early Miocene (Teixell, 1996; Teixell & García-Sansegundo, 1995, and references therein). Uplift associated with this basement thrust can explain the final part of the main cooling phase of sample OB1 and the propagation of deformation ahead of the Alaiž Thrust, through the upper Eocene-lower Oligocene evaporites of the Ebro basin.

In the northern Ebro basin, the regional Barbarin unconformity, dated in the Oligocene-Miocene transition, seals the deformed Cenozoic strata (Riba Arderiu, 1992), essentially marking the end of the Alpine convergence. Since the Miocene, the cooling predicted by QTQt in several models may be influenced by incision of the fluvial networks, as described in other areas of the Pyrenees (Fillon & van der Beek, 2012; García-Castellanos et al., 2003; Jolivet et al., 2007; Labaume, Meresse, Jolivet, & Teixell, 2016; Vergés et al., 2002). However, as samples were at temperatures lower than the PAZ during the Miocene, inverse models are not accurately constrained for this period.

We estimate Eocene exhumation rates and inferred burial of our samples taking into account the weighted mean inverse model obtained and assuming a geothermal gradient of 20–25 °C/km (Bosch et al., 2016; Gómez et al., 2002) and a surface temperature of 10 °C (Table 4). Samples from the Cinco Villas massif (CV1, CV2 without track lengths, and CV3) show exhumation rates ranging between 0.13 and 0.24 km/Myr. The inferred burial estimates at 55 Ma are in the range of 6.4–10.8 km. Sample CV3, the Triassic rock in the western part of the Cinco Villas massif, registered the lowest burial estimates of this group (6.4–8 km) probably due to its geographic location on the border of the massif. Modeling regarding track lengths in CV2 predicts a fast cooling episode between 50 and 40 Ma with an exhumation rate of 0.77 ± 0.08 km/Myr.

Sample LZ2 experienced an exhumation rate of 0.25 ± 0.03 km/Myr during the early Eocene and was buried between 7 and 9 km in the footwall of the Leiza-Aralar Thrust System prior to its exhumation.

East of the PTZ, exhumation rates for the late Eocene in the Oroz-Betelu massif reached 1.12 ± 0.12 km/Myr. At 40 Ma, the inferred burial of the Triassic sample on top of this massif and beneath the Jaca-Pamplona basin was of 7.6–9.5 km. This Mesozoic-Cenozoic sedimentary thickness is similar to or slightly lower than the thickness estimated for that time farther east, in the area uplifted by the Gavarnie thrust (Labaume, Meresse, Jolivet, Teixell, & Lahfid, 2016).

6.4. Integration of the Results in the Framework of the Pyrenean-Cantabrian Mountain Belt

The thermotectonic evolution of the Alpine cycle in the Pyrenean-Cantabrian mountain belt is revealed as a complex history, with the formation of a rift domain of lithospheric hyperextension in several Cretaceous basins and the Cenozoic tectonic inversion of this rift domain resulting in mountain building. During the mid-Cretaceous, a high-temperature thermal event is described in several Pyrenean basins in relation to the formation of a hyperextended rift margin with local mantle exhumation/unroofing (Clerc et al., 2015; Clerc & Lagabriele, 2014; DeFelipe et al., 2017; Tugend et al., 2014). It also implied a high geothermal gradient estimated as high as 80–100 °C/km in the North Pyrenean Zone (Clerc et al., 2014; Hart et al., 2017; Vacherat et al., 2014). This period of high thermal gradient left a thermal imprint in the ZHe thermochronological systems of the South and North Pyrenean Zones (Filleaudeau et al., 2012; Hart et al., 2017). In the Basque-Cantabrian zone, the presence of high-temperature metamorphism, hydrothermalism and remagnetizations during the Cretaceous also implied a high geothermal gradient. However, the high temperatures achieved during hyperextension did not lead to complete resetting of the ZHe system for sample LZ2, collected from a Carboniferous sandstone. This sample was probably located in the hyperthinned domain of the European side of the rift system, far enough from the exhumed mantle domain to escape the strongest thermal effects of the metamorphic aureole, reaching only temperatures of 160–170 °C in the mid-Cretaceous. To the north, complete resetting of the samples in the Cinco Villas massif was probably due to a combination of deep burial and perhaps also high-temperature fluid circulation along the crustal-scale Ollin Fault. This heat source(s) also led to remagnetizations in the Lower Triassic rocks of this massif during the Cretaceous (pre-Turonian; Larrasoana, Parés, del Valle, & Millán, 2003). The sample in the Aldudes massif may have also reached its maximum temperatures in the Late Cretaceous, although they were not as high as temperatures predicted for the samples in the Cinco Villas massif due to a shallower burial under a thinner sedimentary cover.

It is widely accepted that the onset of convergence in the Pyrenees s.s. occurred in the Late Cretaceous, at ~83–84 Ma (Macchiavelli et al., 2017; Teixell et al., 2018, and references therein). At that time, however, oceanic crust was being created in the center of the Bay of Biscay (up to chron A33o, 80 Ma; e.g., Sibuet et al., 2004), implying simultaneous lithospheric extension toward the west. A very detailed kinematic model recently proposed by Macchiavelli et al. (2017) predicts this behavior, with nearly no convergence or extension in the intermediate zone (the Basque-Cantabrian zone) until the beginning of the Eocene. Around the Cinco Villas massif and the Marble Unit, we interpret the high cooling rates observed in the early to middle Eocene as the expression of exhumation by thrusting (curves for LZ2 and CV2 in Figure 8). This period of faster exhumation is observed earlier in the samples from the thin-skinned, north vergent Leiza thrust. It occurred in the early Eocene, by inversion of the former main extensional detachment. The Paleozoic rock sampled is interpreted to be derived from the European paleomargin, wrenched by a secondary structure and incorporated in the Leiza thrust. The samples from the Cinco Villas massif are interpreted to have been buried under several kilometers of Mesozoic sediments under a relatively high geothermal gradient in the mid-Cretaceous. Subsequently, they were cooled by thermal relaxation and later exhumation by the thick-skinned, south vergent Ollin Fault with a major pulse in the middle Eocene, postdating the movement of the Leiza thrust, as also deduced from field observations (Martínez-Torres, 2008).

East of the PTZ, the sample from the Oroz-Betelu massif shows evidence of rapid exhumation by thrusting in the late Eocene. Before that, the massif experienced continuous but slow heating that must be related to sedimentary burial. Although the *t-T* path for this sample is not particularly well constrained, it is noteworthy that it shows an acceleration of heating (burial) since the late Ypresian, which corresponds to the onset of turbidite deposition in the Jaca-Pamplona basin, with sediments coming at that stage from uplifted areas toward the east (e.g., Teixell & García-Sansegundo, 1995). The rapid exhumation of the Oroz-Betelu massif in the late Eocene, interpreted here to be related to the emplacement of the Gavarnie thrust, is coherent with the general tectonic evolution of the South Pyrenean Zone.

In the West-Central Pyrenees, exhumation in the South Pyrenean Zone migrated southward along south vergent basement thrusts from the early Eocene to the late Oligocene-early Miocene in a normal propagation sequence (Labaume, Meresse, Jolivet, Teixell, & Lahfid, 2016; Teixell, 1998). AFT ages increase southward and stratigraphically upward, reflecting the progressive southward decrease in the level of fission-track

resetting, from totally reset Paleozoic and lower Eocene rocks to weak or no resetting in the upper Eocene-Oligocene rocks (Labaume, Meresse, Jolivet, Teixell, & Lahfid, 2016).

In the North Pyrenean Zone of the West-Central Pyrenees, the period of rapid exhumation through the PAZ started in the middle Eocene, migrated southward across the Axial Zone during the late Eocene and early Oligocene in relation to the activation of the Gavarnie and Guarga thrusts, and slowed down during the late Oligocene-early Miocene (Labaume, Meresse, Jolivet, & Teixell, 2016). Inverse modeling for the sample from the Alduides massif did not provide reliable results. The forward modeling for the ZHe ages, on the other hand, suggests that its evolution is compatible with slow cooling in the Late Cretaceous related to decay of the thermal anomaly followed by tectonic uplift with an accelerated cooling phase. Labaume, Meresse, Jolivet, and Teixell (2016) also found a pulse of accelerated cooling in the Miocene for the southern part of the western termination of the Axial Zone, which they attribute to late tectonic uplift related to a pop-up basement structure activated coevally with, or slightly after, the end of shortening at the Pyrenean mountain fronts. A similar late tectonic movement might be envisaged for the Alduides massif (Figure 6f), although we must note again the loose constraints of our data.

Regarding the exhumation rates, our results contribute by depicting more clearly a general decrease in the inferred maximum values from the central Pyrenees toward the west. Maximum exhumation rates recorded in the Axial Zone range between 1 and 4 km/Myr for the late Eocene and early Oligocene, and decreases strongly at circa 30 Ma (Fillon & van der Beek, 2012; Fitzgerald et al., 1999; Gibson et al., 2007; Whitchurch et al., 2011). Our results for the western Pyrenees–eastern Cantabrian Mountains (considering the modeling of CV2 with track length data representative of the whole Cinco Villas massif) lie between 0.25 and 1.12 km/Myr. In the central Cantabrian Mountains, Fillon et al. (2016) estimated exhumation rates of 0.24–0.30 km/Myr between 39 and 29 Ma. Finally, in the western Cantabrian Mountains, Cenozoic exhumation rates are as low as 0.02–0.06 km/Myr (Grobe et al., 2010; Martín-González et al., 2012).

After the period of rapid orogenic exhumation during the Eocene-Oligocene, exhumation rates slowed and deformation propagated south of the Alaiz Thrust. During the Miocene (at 13–8.5 Ma), opening of the Ebro basin to the Mediterranean Sea caused subsequent re-excavation and valley incision of the southern Pyrenees (García-Castellanos et al., 2003). This fluvial incision left a thermal imprint in the thermochronological systems of samples in the Axial Zone and the South Pyrenean Central Unit (Beamud et al., 2011; Bosch et al., 2016; Fillon et al., 2013; Jolivet et al., 2007; Labaume, Meresse, Jolivet, & Teixell, 2016). In the westernmost Pyrenees, samples AL1 and OB1 were located in the catchment of the Ebro River and only AL1 may have experienced a significant Miocene cooling (Figure 6). This cooling, which is poorly constrained, could also be related to late orogenic activation of the Roncesvalles Thrust, proposed for the western termination of the Axial Zone (Labaume, Meresse, Jolivet, & Teixell, 2016). The lack of a strong and generalized signature of Miocene cooling is not surprising in this part of the belt due to the lower altitudes and longer distance to the river base level as compared to other areas of the Pyrenees.

7. Conclusions

We report here a new low-temperature thermochronological data set based on AFT and ZHe dating for the Basque massifs and surroundings, which previously represented a significant data gap in the Pyrenean-Cantabrian mountain belt. This new data set allows us to reexamine the evolution of basement rocks in the Pyrenees from the rift-related Mesozoic hyperextension to the Cenozoic tectonic inversion.

AFT central ages cluster around the Eocene-Oligocene, but ZHe ages are more dispersed. The samples of this study can be separated into two groups according to the ZHe age-eU correlations of the zircons analyzed in each sample: Group 1 includes samples from the Cinco Villas massifs (CV1, CV2, and CV3) with clustered ZHe age-eU values and Group 2 includes samples from the Alduides massif and from a Paleozoic rock in the Leiza thrust (AL1 and LZ2, respectively) with dispersed ZHe ages and eU values. ZHe ages for Group 1 point to total resetting of the ZHe system during the Alpine orogeny, while samples belonging to Group 2 are partially reset. A sample from the Oroz-Betelu massif shows an intermediate behavior, pointing to a partially reset system.

The existence of partially reset ZHe ages, together with forward and inverse modeling, provides information on the thermal inheritance of our samples and the maximum temperature achieved before their Alpine

exhumation. The Cretaceous hyperextension led to a thermal anomaly in the eastern Basque-Cantabrian basin and to the high-temperature metamorphism of the Marble Unit, especially in its eastern part, close to the PTZ. This metamorphism did not lead to a total resetting of the ZHe thermochronometer in sample LZ2, which crops out in the western part of the Marble Unit, in a basement slice uplifted by the inversion of the Leiza detachment system. Therefore, we interpret this sample to have been located in the footwall of the Leiza detachment system in the European margin during the Cretaceous, at some distance from the exhumed/unroofed mantle domain. Inverse modeling shows that samples from the Cinco Villas massif, even farther from the exhumed/unroofed mantle domain reached maximum temperatures of ~240–280 °C during the Late Cretaceous. We therefore infer that the Paleozoic basement was deeply buried so that high temperatures and perhaps hot fluid circulation also led to remagnetizations in the Triassic rocks laying on top of this massif. The rest of the samples reached maximum temperatures of ~190–220 °C prior to fast cooling by tectonic uplift in the early Eocene (Leiza thrust), early-mid-Eocene (Cinco Villas massif) and late Eocene (Oroz-Betelu massif).

Samples in the Cinco Villas and Alduides massifs were cooled from 100–80 Ma to the present, although an inverse model including track lengths in the Cinco Villas massif predicted cooling since the early Eocene. Estimated Eocene exhumation rates based on the inverse modeling results for samples in the Cinco Villas massif, show values of 0.13–0.24 km/Myr. Inverse modeling for sample CV2 including track lengths predicts an exhumation rate of 0.77 km/Myr between 50 and 40 Ma, coinciding with the start of an episode of fast cooling dated around 50 Ma farther east, along the Lakora basement thrust. The sample located along the Leiza thrust (LZ2) was wrenched from the European basement, incorporated in a tectonic slice, and consequently exhumed at a rate of 0.25 km/Myr between 55 and 45 Ma. Inverse modeling also shows that this sample experienced a period of slow cooling since 45 Ma, suggesting that the Cinco Villas massif was exhumed over the Central Depression and Marble Unit. The sample from the Oroz-Betelu massif reached maximum temperatures at 40 Ma, when it reached its maximum burial depth below the synorogenic sediments of the Jaca-Pamplona basin and experienced a relatively rapid exhumation at a rate of 1.12 km/Myr between 40 and 34 Ma in the hanging wall of the Gavarnie thrust. Eocene burial estimates for samples in the Paleozoic rock pinned along the Leiza thrust, and the Cinco Villas and Oroz-Betelu massifs range between 6.4 and 12.5 km. The Alpine orogeny led to the inversion of the Cretaceous basins and extensional structures and overall uplift of the Mesozoic basins, thus closing the thermochronological systems in the Cenozoic.

This study highlights the relevance of combining AFT and ZHe dating, fission track length measurements, and modeling with structural constraints to unravel the extensional and contractional history of an orogenic belt. With this information, a more precise reconstruction of the Alpine orogeny in the Basque-Cantabrian zone has been established. The integration of results from adjacent parts of the Pyrenean-Cantabrian mountain belt offers a coherent picture in which the most rapid exhumation phase took place essentially during the Eocene and Oligocene, although at rates that decreases in an east to west direction, from the Pyrenees to the Cantabrian Mountains.

Acknowledgments

This is a contribution of the GEOTEC Group (IDI/2018/000216) and Projects MISTERIOS (CGL2013-48601-C2-2-R), Consolider-Ingenio 2010 TOPO-IBERIA (CSD2006-00041), and ESF TopoEurope Project PYRTEC (SV-PA-10-03-IP2-PYRTEC). We thank additional financial support by the University of Oviedo-Banco Santander, the Government of the Principality of Asturias through the Science, Technology and Innovation Plan (PCTI), the European Union through FEDER funds, and the Spanish Ministry of Education, Culture and Sport through the Training Programme for Academic Staff (FPU Grant for Irene DeFelipe). Two anonymous reviewers are greatly acknowledged for their useful and constructive comments. Full AFT and ZHe data set is available in the DIGITAL.CSIC repository (DeFelipe et al., 2019). Email address for correspondence: irene.defelipe@gmail.com.

References

- Ábalos, B. (2016). Geological map of the Basque-Cantabrian Basin and a new tectonic interpretation of the Basque Arc. *International Journal of Earth Sciences*, 105(8), 2327–2354. <https://doi.org/10.1007/s00531-016-1291-6>
- Abd Elmola, A., Buatier, M., Monié, P., Labaume, P., Trap, P., & Charpentier, D. (2018). ⁴⁰Ar/³⁹Ar muscovite dating of thrust activity: A case study from the Axial Zone of the Pyrenees. *Tectonophysics*, 745, 412–429. <https://doi.org/10.1016/j.tecto.2018.09.004>
- Alonso, J. L., Pulgar, J. A., García-Ramos, J. C., & Barba, P. (1996). Tertiary basins and Alpine tectonics in the Cantabrian Mountains (NW Spain). In P. F. Friend, & C. J. Dabrio (Eds.), *Tertiary basins of Spain: The stratigraphic record of crustal kinematics* (pp. 214–227). Cambridge: Cambridge University Press.
- Arostegui, J., Ramón-Lluch, R., Martínez-Torres, L. M., & Eguiluz, L. (1987). Contribución de los minerales de la arcilla a la diferenciación de las placas ibérica y europea en el Pirineo vasco. *Geogaceta*, 2, 34–36.
- Aurell, M., Robles, S., Bádenas, B., Rosales, I., Quesada, S., Meléndez, G., & García-Ramos, J. C. (2003). Transgressive–regressive cycles and Jurassic palaeogeography of northeast Iberia. *Sedimentary Geology*, 162(3–4), 239–271. [https://doi.org/10.1016/S0037-0738\(03\)00154-4](https://doi.org/10.1016/S0037-0738(03)00154-4)
- Bádenas, B. (1996). El jurásico superior de la sierra de Aralar (Guipúzcoa y Navarra): Caracterización sedimentológica y paleogeográfica. *Estudios Geológicos*, 52, 147–160.
- Barbarand, J., Hurford, T., & Carter, A. (2003). Variation in apatite fission-track length measurement: Implications for thermal history modelling. *Chemical Geology*, 198(1–2), 77–106. [https://doi.org/10.1016/S0009-2541\(02\)00423-0](https://doi.org/10.1016/S0009-2541(02)00423-0)
- Barnett-Moore, N., Font, E., & Neres, M. (2017). A reply to the comment on “Assessing discrepancies between previous plate kinematic models of Mesozoic Iberia and their constraints” by Barnett-Moore et al. *Tectonics*, 36, 3286–3297. <https://doi.org/10.1002/2017TC00476>

- Barnett-Moore, N., Hosseinpour, M., & Maus, S. (2016). Assessing discrepancies between previous plate kinematic models of Mesozoic Iberia and their constraints. *Tectonics*, 35, 1843–1862. <https://doi.org/10.1002/2015TC004019>
- Barnett-Moore, N., Müller, D. R., Williams, S., Skogseid, J., & Seton, M. (2018). A reconstruction of the North Atlantic since the earliest Jurassic. *Basin Research*, 30, 160–185. <https://doi.org/10.1111/bre.12214>
- Barnolas, A., & Gil-Peña, I. (2001). Ejemplos de relleno sedimentario multiepisdico en una cuenca de antepais fragmentada: La Cuenca Surpirenaica. *Boletín Geológico y Minero*, 112(3), 17–38.
- Barnolas, A., & Teixell, A. (1994). Platform sedimentation and collapse in a carbonate-dominated margin of a foreland basin (Jaca Basin, Eocene, Southern Pyrenees). *Geology*, 22(12), 1107–1110. [https://doi.org/10.1130/0091-7613\(1994\)022<1107:PSACIA>2.3.CO;2](https://doi.org/10.1130/0091-7613(1994)022<1107:PSACIA>2.3.CO;2)
- Beamud, E., Muñoz, J. A., Fitzgerald, P. G., Baldwin, S. L., Garcés, M., Cabrera, L., & Metcalf, J. R. (2011). Magnetostratigraphy and detrital apatite fission track thermochronology in syntectonic conglomerates: Constraints on the exhumation of the South-Central Pyrenees. *Basin Research*, 23(3), 309–331. <https://doi.org/10.1111/j.1365-2117.2010.00492.x>
- Beaumont, C., Muñoz, J. A., Hamilton, J., & Fullsack, P. (2000). Factors controlling the Alpine evolution of the central Pyrenees inferred from a comparison of observations and geodynamical models. *Journal of Geophysical Research*, 105(B4), 8121–8145. <https://doi.org/10.1029/1999JB900390>
- Bodego, A., Iriarte, E., Agirrezabala, L. M., García-Mondéjar, J., & López-Horgue, M. A. (2015). Synextensional mid-Cretaceous stratigraphic architecture of the eastern Basque–Cantabrian basin margin (western Pyrenees). *Cretaceous Research*, 55, 229–261. <https://doi.org/10.1016/j.cretres.2015.01.006>
- Bodego, A., Iriarte, E., López-Horgue, M. A., & Álvarez, I. (2018). Rift-margin extensional forced folds and salt tectonics in the eastern Basque–Cantabrian rift basin (western Pyrenees). *Marine and Petroleum Geology*, 91, 667–682. <https://doi.org/10.1016/j.marpetgeo.2018.02.007>
- Bosch, G., Teixell, A., Jolivet, M., Labaume, P., Stockli, D., Domènech, M., & Monié, P. (2016). Timing of Eocene–Miocene thrust activity in the Western Axial Zone and Châinons Béarnais (west-central Pyrenees) revealed by multi-method thermochronology. *Comptes Rendus Geoscience*, 348(3–4), 246–256. <https://doi.org/10.1016/j.crte.2016.01.001>
- Brandon, M. T. (2002). Decomposition of mixed age distributions using Binomfit. *Track*, 24, 13–18.
- Brandon, M. T. (2005). BinomFit: A windows program for estimating fission-track ages for concordant and mixed gran age distribution.
- Brusset, S., Déramond, J., & Souquet, P. (1997). Évolution tectono-sédimentaire des bassins flexurés profonds et à taux de sédimentation réduit: Exemple du bassin de flysch de Saint-Jean-de-Luz (Pyrénées-Atlantiques, France) au Crétacé supérieur. *Comptes Rendus de l'Académie Des Sciences-Series IIA-Earth and Planetary Science*, 325, 265–271. [https://doi.org/10.1016/S1251-8050\(97\)88299-7](https://doi.org/10.1016/S1251-8050(97)88299-7)
- Campos, J. (1979). Estudio geológico del Pirineo vasco al W del río Bidasoa. Sociedad de Ciencias Naturales Aranzadi, Numero 1-2, 3–139.
- Campos, J., & García-Dueñas, V. (1972). Mapa Geológico de España E. 1:50.000. Hoja 64, San Sebastián. Instituto Geológico y Minero de España, IGME.
- Campos, J., García-Dueñas, V., Solé, J., & Villalobos, L. (1975). Memoria del Mapa Geológico de España E. 1:50.000. Hoja 65, Vera de Bidasoa. Instituto Geológico y Minero de España, IGME.
- Carbayo, A., del Valle, J., León, L., & Villalobos, L. (1972). Mapa Geológico de España E. 1:50.000. Hoja 116, Garralda. Instituto Geológico y Minero de España, IGME.
- Carbayo, A., León, L., & Villalobos, L. (1977). Mapa Geológico de España E. 1:50.000. Hoja 115, Gulina. Instituto Geológico y Minero de España, IGME.
- Carlson, W. D., Donelick, R. A., & Ketcham, R. A. (1999). Variability of apatite fission-track annealing kinetics: I. Experimental results. *American Mineralogist*, 84(9), 1213–1223. <https://doi.org/10.2138/am-1999-0901>
- Carrière, K. L. (2006). Neoproterozoic to Holocene tectonothermal evolution of the southern Cantabrian Mountains NW Iberia, revealed by apatite fission-track thermochronology, (Phd Thesis). <https://doi.org/10.11588/heidok.00006664>
- Castañares, L. M., Robles, S., Gimeno, D., & Bravo, J. C. V. (2001). The submarine volcanic system of the Errigoiti Formation (Albian–Santonian of the Basque–Cantabrian Basin, Northern Spain): Stratigraphic framework, facies, and sequences. *Journal of Sedimentary Research*, 71, 318–333. <https://doi.org/10.1306/080700710318>
- Ceriani, A., Di Giulio, A., Fantoni, R., & Scotti, P. (2006). Cooling in rift sequences during increasing burial depth due to heat flow decrease. *Terra Nova*, 18(5), 365–371. <https://doi.org/10.1111/j.1365-3121.2006.00700.x>
- Choukroune, P., & ECORS Team (1989). The ECORS Pyrenean deep seismic profiles reflection data and the overall structure of an orogenic belt. *Tectonics*, 8(1), 23–39. <https://doi.org/10.1029/TC008i001p00023>
- Clerc, C., Boulvais, P., Lagabrielle, Y., & de Saint Blanquat, M. (2014). Ophealcites from the northern Pyrenean belt: A field, petrographic and stable isotope study. *International Journal of Earth Sciences*, 103(1), 141–163. <https://doi.org/10.1007/s00531-013-0927-z>
- Clerc, C., & Lagabrielle, Y. (2014). Thermal control on the modes of crustal thinning leading to mantle exhumation: Insights from the Cretaceous Pyrenean hot paleomargins. *Tectonics*, 33, 1340–1359. <https://doi.org/10.1002/2013TC003471>
- Clerc, C., Lahfid, A., Monié, P., Lagabrielle, Y., Chopin, C., Poujol, M., et al. (2015). High-temperature metamorphism during extreme thinning of the continental crust: A reappraisal of the North Pyrenean passive paleomargin. *Solid Earth*, 6(2), 643–668. <https://doi.org/10.5194/se-6-643-2015>
- Coney, P. J., Muñoz, J. A., McClay, K. R., & Evenchick, C. A. (1996). Syntectonic burial and post-tectonic exhumation of the southern Pyrenees foreland fold-thrust belt. *Journal of the Geological Society, London*, 153(1), 9–16. <https://doi.org/10.1144/gsjgs.153.1.0009>
- Costa, E., Garcés, M., López-Blanco, M., Beamud, E., Gómez-Paccard, M., & Larrasoana, J. C. (2010). Closing and continentalization of the South Pyrenean foreland basin (NE Spain): Magnetochronological constraints. *Basin Research*, 22, 904–917. <https://doi.org/10.1111/j.1365-2117.2009.00452.x>
- DeFelipe, I., Pedreira, D., Pulgar, J. A., Iriarte, E., & Mendia, M. (2017). Mantle exhumation and metamorphism in the Basque–Cantabrian Basin (N Spain). Stable and clumped isotopic analysis in carbonates and comparison with ophealcites in the North–Pyrenean Zone (Urdach and Lherz). *Geochemistry, Geophysics, Geosystems*, 18, 631–652. <https://doi.org/10.1002/2016GC006690>
- DeFelipe, I., Pedreira, D., Pulgar, P., van der Beek, P., Bernet, M., & Pik, R. (2019). Apatite fission track and zircon (U–Th)/He dataset in the eastern Basque–Cantabrian Zone–western Pyrenees. <https://doi.org/10.20350/digitalCSIC/8643>
- DeFelipe, I., Pulgar, J. A., & Pedreira, D. (2018). Crustal structure of the Eastern Basque–Cantabrian Zone/western Pyrenees: From the Cretaceous hyperextension to the Cenozoic inversion. *Revista de la Sociedad Geológica de España*, 31(2), 69–82. ISSN 2255-1379.
- Del Rio, P., Barbero, L., & Stuart, F. M. (2009). Exhumation of the Sierra de Cameros (Iberian Range, Spain): Constraints from low-temperature thermochronology. *Geological Society, London, Special Publications*, 324(1), 153–166. <https://doi.org/10.1144/SP324.12>
- Del Valle, H.F., Müller, D., Requadt, H., Campos, J., García-Dueñas, V., Garrote, A., et al. (1972). Mapa Geológico de España E. 1:50.000. Hoja 65, Vera de Bidasoa. Instituto Geológico y Minero de España, IGME.
- Del Valle, J. (1974). Mapa Geológico de España E. 1:50.000. Hoja 141, Pamplona. Instituto Geológico y Minero de España, IGME.

- Del Valle, J., Villalobos, L., Bornhorst, A., de Boer, H. U., Krauss, H. F., Mohr, K., et al. (1973). Mapa Geológico de España E. 1:50.000. Hoja 90, Sumbilla. Instituto Geológico y Minero de España, IGME.
- Diez, B., Broutin, J., & Ferrer, J. (2005). Difficulties encountered in defining the Permian–Triassic boundary in Buntsandstein facies of the western Peritethyan domain based on palynological data. *Palaeogeography, Palaeoclimatology, Palaeoecology*, 229, 40–53. <https://doi.org/10.1016/j.palaeo.2005.06.029>
- Donelick, R. A., O'Sullivan, P. B., & Ketcham, R. A. (2005). Apatite fission-track analysis. *Reviews in Mineralogy and Geochemistry*, 58(1), 49–94. <https://doi.org/10.2138/rmg.2005.58.3>
- Ducoux, M., Jolivet, L., Gumiaux, C., Baudin, T., Cagnard, F., Masini, E., & Lahfid, A. (2018). Unravelling early orogenic processes: Constraints from the inverted hyper-extended rift preserved in the Basco-Cantabrian belt. *Geophysical Research Abstracts*, vol. 20, EGU2018-19143.
- Fernández, M., Marzán, I., Correia, A., & Ramalho, E. (1998). Heat flow, heat production, and lithospheric thermal regime in the Iberian Peninsula. *Tectonophysics*, 291(1-4), 29–53. [https://doi.org/10.1016/S0040-1951\(98\)00029-8](https://doi.org/10.1016/S0040-1951(98)00029-8)
- Filleaudeau, P.-Y., Mouthereau, F., & Pik, R. (2012). Thermo-tectonic evolution of the south-central Pyrenees from rifting to orogeny: Insights from detrital zircon U/Pb and (U-Th)/He thermochronometry. *Basin Research*, 24, 401–417. <https://doi.org/10.1111/j.1365-2117.2011.00535.x>
- Fillon, C., Gautheron, C., & van der Beek, P. (2013). Oligocene-Miocene burial and exhumation of the Southern Pyrenean foreland quantified by low-temperature thermochronology. *Journal of the Geological Society, London*, 170(1), 67–77. <https://doi.org/10.1144/jgs2012-051>
- Fillon, C., Pedreira, D., van der Beek, P. A., Huismans, R. S., Barbero, L., & Pulgar, J. A. (2016). Alpine exhumation of the central Cantabrian Mountains, Northwest Spain. *Tectonics*, 35, 339–356. <https://doi.org/10.1002/2015TC004050>
- Fillon, C., & van der Beek, P. (2012). Post-orogenic evolution of the southern Pyrenees: Constraints from inverse thermo-kinematic modelling of low-temperature thermochronology data. *Basin Research*, 24(4), 418–436. <https://doi.org/10.1111/j.1365-2117.2011.00533.x>
- Fitzgerald, P. G., Muñoz, J. A., Coney, P. J., & Baldwin, S. L. (1999). Asymmetric exhumation across the Pyrenean orogen: Implications for the tectonic evolution of a collisional orogen. *Earth and Planetary Science Letters*, 173(3), 157–170. [https://doi.org/10.1016/S0012-821X\(99\)00225-3](https://doi.org/10.1016/S0012-821X(99)00225-3)
- Flowers, R. M., Farley, K. A., & Ketcham, R. A. (2015). A reporting protocol for thermochronologic modeling illustrated with data from the Grand Canyon. *Earth and Planetary Science Letters*, 432, 425–435. <https://doi.org/10.1016/j.epsl.2015.09.053>
- Flowers, R. M., Farley, K. A., & Ketcham, R. A. (2016). Response to comment on “A reporting protocol for thermochronologic modeling illustrated with data from the Grand Canyon”. *Earth and Planetary Science Letters*, 441, 213. <https://doi.org/10.1016/j.epsl.2016.02.024>
- Gabaldón, V., Campos Fernández, J., Olivé Davó, A., Ramírez Merino, J., Solé Sedó, J., & Villalobos Vilches, L. (1983). Mapa Geológico de España E. 1:50.000. Hoja 89, Tolosa. Instituto Geológico y Minero de España, IGME.
- Gabaldón, V., Ramírez Merino, J., Olivé Davó, A., Villalobos Vilches, L., León González, L., & Carbayo Olivares, A. (1984). Mapa Geológico de España E. 1:50.000. Hoja 114, Alsasua. Instituto Geológico y Minero de España, IGME.
- Galbraith, R. F. (1990). The radial plot: Graphical assessment of spread in ages. *Nuclear Tracks and Radiation Measurements*, 17(3), 207–214. [https://doi.org/10.1016/1359-0189\(90\)90036-W](https://doi.org/10.1016/1359-0189(90)90036-W)
- Galbraith, R. F., & Laslett, G. M. (1993). Statistical models for mixed fission track ages. *Nuclear Tracks and Radiation Measurements*, 21(4), 459–470. [https://doi.org/10.1016/1359-0189\(93\)90185-C](https://doi.org/10.1016/1359-0189(93)90185-C)
- Gallagher, K. (2012). Transdimensional inverse thermal history modeling for quantitative thermochronology. *Journal of Geophysical Research*, 117, B02408. <https://doi.org/10.1029/2011JB008825>
- Gallagher, K. (2016). Comment on ‘A reporting protocol for thermochronologic modeling illustrated with data from the Grand Canyon’ by Flowers, Farley & Ketcham. *Earth and Planetary Science Letters*, 441, 211–212. <https://doi.org/10.1016/j.epsl.2016.02.021>
- Gallagher, K., & Ketcham, R. A. (2018). Comment on “Thermal history modelling: HeFTy vs. QTQt” by Vermeesch and Tian. *Earth-Science Reviews*, 176, 387–394. <https://doi.org/10.1016/j.earscirev.2017.11.001>
- Gallastegui, J., Pulgar, J. A., & Gallart, J. (2002). Initiation of an active margin at the North Iberian continent-ocean transition. *Tectonics*, 21(4), 1033. <https://doi.org/10.1029/2001TC901046>
- García-Castellanos, D., Vergés, J., Gaspar-Escribano, J., & Cloetingh, S. (2003). Interplay between tectonics, climate, and fluvial transport during the Cenozoic evolution of the Ebro Basin (NE Iberia). *Journal of Geophysical Research*, 108(B7), 2347. <https://doi.org/10.1029/2002JB002073>
- García-Mondéjar, J., Agirrezabala, L. M., Aranburu, A., Fernández-Mendiola, P. A., Gómez-Pérez, I., López-Horgue, M., & Rosales, I. (1996). Aptian-Albian Tectonic pattern of the Basque-Cantabrian Basin (northern Spain). *Geological Journal*, 31(1), 13–45. [https://doi.org/10.1002/\(SICI\)1099-1034\(199603\)31:1<13::AID-GJ689>3.0.CO;2-Y](https://doi.org/10.1002/(SICI)1099-1034(199603)31:1<13::AID-GJ689>3.0.CO;2-Y)
- García-Sansegundo, J., & Barnolas, A. (2000). La terminación occidental del cabalgamiento de la Sierra de Illón (Pirineos Navarros, España). *Geo-Temas*, 1(2), 93–96.
- Gibson, M., Sinclair, H. D., Lynn, G. J., & Stuart, F. M. (2007). Late- to post-orogenic exhumation of the Central Pyrenees revealed through combined thermochronological data and modelling. *Basin Research*, 19, 323–334. <https://doi.org/10.1111/j.1365-2117.2007.00333.x>
- Godard, V., Pik, R., Lavée, J., Cattin, R., Tibari, B., de Sigoyer, J., et al. (2009). Late Cenozoic evolution of the central Longmen Shan, Eastern Tibet: Insight from (U-Th)/He thermochronometry. *Tectonics*, 28, TC5009. <https://doi.org/10.1029/2008TC002407>
- Gómez, M., Vergés, J., & Ríaza, C. (2002). Inversion tectonics of the northern margin of the Basque Cantabrian Basin. *Bulletin de la Société Géologique de France*, 173(5), 449–459. <https://doi.org/10.2113/173.5.449>
- González, C., Valverde, I., & Lafuente, A. L. (2007). Mineralogical and geo-chemical characterization of a diapiric formation in the North of Spain. *Catena*, 70(3), 375–387. <https://doi.org/10.1016/j.catena.2006.11.005>
- Grobe, R. W., Álvarez-Marrón, J., Glasmacher, U. A., & Menéndez-Duarte, R. (2010). Low temperature exhumation history of Variscan-age rocks in the western Cantabrian Mountains (NW Spain) recorded by apatite fission-track data. *Tectonophysics*, 489(1-4), 76–90. <https://doi.org/10.1016/j.tecto.2010.04.006>
- Grobe, R. W., Álvarez-Marrón, J., Glasmacher, U. A., & Stuart, F. M. (2014). Mesozoic exhumation history and palaeolandscape of the Iberian Massif in eastern Galicia from apatite fission-track and (U+Th)/He data. *International Journal of Earth Sciences*, 103(2), 539–561. <https://doi.org/10.1007/s00531-013-0976-3>
- Guenther, W. R., Reiners, P. W., Decelles, P. G., & Kendall, J. (2015). Sevier belt exhumation in central Utah constrained from complex zircon (U-Th)/He data sets: Radiation damage and He inheritance effects on partially reset detrital zircons. *Bulletin Geological Society of America*, 127(3-4), 323–348. <https://doi.org/10.1130/B31032.1>

- Guenther, W. R., Reiners, P. W., Ketcham, R. A., Nasdala, L., & Giester, G. (2013). Helium diffusion in natural zircon: Radiation damage, anisotropy, and the interpretation of zircon (U-Th)/He thermochronology. *American Journal of Science*, 313(3), 145–198. <https://doi.org/10.2475/03.2013.01>
- Hart, N. R., Stockli, D. F., Lavier, L. L., & Hayman, N. W. (2017). Thermal evolution of a hyperextended rift basin, Mauléon Basin, western Pyrenees. *Tectonics*, 36, 1103–1128. <https://doi.org/10.1002/2016TC004365>
- Iriarte, E. (2004). La Depresión Intermedia entre Leiza y Elizondo (Pirineo Occidental): Estratigrafía y reñaciones tectónica-sedimentación durante el Cretácico. Tesis Doctoral Inédita. Universidad del País Vasco, 310 pp.
- Iriarte, E., López-Horgue, A., Aramburu, A., Bodego, A., Cerani, A., & García-Mondéjar, J. (2011). Synsedimentary Cretaceous hydrothermalism in the Leiza fault (Basque-Cantabrian Basin, western Pyrenees). 23ème Réunion des Sciences de la Terre, Bordeaux. ISBN: 2-85363-096-X.
- Jammes, S., Huismans, R. S., & Muñoz, J. A. (2014). Lateral variation in structural style of mountain building: controls of rheological and rift inheritance. *Terra Nova*, 26, 201–207. <https://doi.org/10.1111/ter.12087>
- Jammes, S., Manatschal, G., Lavier, L., & Masini, E. (2009). Tectonosedimentary evolution related to extreme crustal thinning ahead of a propagating ocean: Example of the western Pyrenees. *Tectonics*, 28, TC4012. <https://doi.org/10.1029/2008TC002406>
- Jolivet, M., Labaume, P., Monié, P., Brunel, M., Arnaud, N., & Campani, M. (2007). Thermochronology constraints for the propagation sequence of the south Pyrenean basement thrust system (France-Spain). *Tectonics*, 26, TC5007. <https://doi.org/10.1029/2006TC002080>
- Juez-Larré, J., & Andriessen, P. A. M. (2006). Tectonothermal evolution of the northeastern margin of Iberia since the break-up of Pangea to present, revealed by low-temperature fission-track and (U-Th)/He thermochronology. A case history of the Catalan Coastal Ranges. *Earth and Planetary Science Letters*, 243(1-2), 159–180. <https://doi.org/10.1016/j.epsl.2005.12.026>
- Ketcham, R. A. (2005). Forward and inverse modeling of low-temperature thermochronometry data. In P. W. Reiners, & T. A. Ehlers (Eds.), *Low-Temperature Thermochronology: Techniques, Interpretations, and Applications, Reviews in Mineralogy and Geochemistry* (Vol. 58, pp. 275–314). Washington DC: Mineralogical Society of America.
- Ketcham, R. A., Carter, A., Donelick, R. A., Barbarand, J., & Hurford, A. J. (2007). Improved measurement of fission-track annealing in apatite using c-axis projection. *American Mineralogist*, 92(5-6), 789–798. <https://doi.org/10.2138/am.2007.2280>
- Ketcham, R. A., Gautheron, C., & Tassan-Got, L. (2011). Accounting for long alpha-particle stopping distances in (U-Th-Sm)/He geochronology: Refinement of the baseline case. *Geochimica et Cosmochimica Acta*, 75(24), 7779–7791. <https://doi.org/10.1016/j.gca.2011.10.011>
- Knausse, H. F., Müller, D., Requadt, H., Campos, J., García-Dueñas, V., Garrote, A., et al. (1972). *Mapa Geológico de España 1:50.000, hoja nº 65 (Vera de Bidasoa)*. Madrid: IGME.
- Kohn, B., Ling, C., & Gleadow, A. (2018). Fission-Track Analysis: Field Collection, Sample Preparation and Data Acquisition. In M. Malusa, & P. Fitzgerald (Eds.), *Fission-Track Thermochronology and its Application to Geology* (pp. 25–48). Berlin: Springer.
- Labaume, P., Meresse, F., Jolivet, M., & Teixell, A. (2016). Exhumation sequence of the basement thrust units in the west-central Pyrenees. Constraints from apatite fission track analysis. *Geogaceta. Sociedad Geológica de España*, 60, 11–14.
- Labaume, P., Meresse, F., Jolivet, M., Teixell, A., & Lahfid, A. (2016). Tectonothermal history of an exhumed thrust-sheet-top basin: An example from the south Pyrenean thrust belt. AGU Publications. *Tectonics*, 35, 1280–1313. <https://doi.org/10.1002/2016TC004192>
- Labaume, P., Séguret, M., & Seyve, C. (1985). Evolution of a turbiditic foreland basin and analogy with an accretionary prism: Example of the Eocene South-Pyrenean basin. *Tectonics*, 4(7), 661–685. <https://doi.org/10.1029/TC004i007p00661>
- Labaume, P., & Teixell, A. (2018). 3D structure of subsurface thrusts in the eastern Jaca Basin, southern Pyrenees. *Geologica Acta*, 16(4), 477–498. <https://doi.org/10.1344/GeologicaActa2018.16.4.9>
- Lagabriele, Y., & Bodinier, J.-L. (2008). Submarine reworking of exhumed subcontinental mantle rocks: Field evidence from the Lherz peridotites, French Pyrenees. *Terra Nova*, 20, 11–21. <https://doi.org/10.1111/j.1365-3121.2007.00781.x>
- Lagabriele, Y., Labaume, P., & de Saint Blanquat, M. (2010). Mantle exhumation, crustal denudation, and gravity tectonics during Cretaceous rifting in the Pyrenean realm (SW Europe): Insights from the geological setting of the Iherzolite bodies. *Tectonics*, 29, TC4012. <https://doi.org/10.1029/2009TC002588>
- Lamare, P. (1936). Recherches géologiques dans le Pyrénées basques d'Espagne. *Mém. Soc. Géol. France. nouv. Sér.* II-27.
- Lanaja, J. M. (1987). Contribución de la exploración petrolífera al conocimiento de la geología de España. (I. G. y M. de España, Ed.).
- Larrasoaña, J. C., Parés, J. M., del Valle, J., & Millán, H. (2003). Triassic paleomagnetism from the Western Pyrenees revisited: Implications for the Iberian–Eurasian Mesozoic plate boundary. *Tectonophysics*, 362(1-4), 161–182. [https://doi.org/10.1016/S0040-1951\(02\)00636-4](https://doi.org/10.1016/S0040-1951(02)00636-4)
- Larrasoaña, J. C., Parés, J. M., Millán, H., del Valle, J., & Pueyo, E. L. (2003). Paleomagnetic, structural, and stratigraphic constraints on transverse fault kinematics during basin inversion: The Pamplona Fault (Pyrenees, north Spain). *Tectonics*, 22(6), 1071. <https://doi.org/10.1029/2002TC001446>
- Macchiavelli, C., Vergés, J., Schettino, A., Fernández, M., Turco, E., Casciello, E., et al. (2017). A new southern North Atlantic isochron map: Insights into the drift of the Iberian plate since the Late Cretaceous. *Journal of Geophysical Research: Solid Earth*, 122, 9603–9626. <https://doi.org/10.1002/2017JB014769>
- Martínez-Torres, L. M. (2008). El Manto de los Mármoles (Pirineo Occidental): Geología estructural y evolución geodinámica. Tesis doctoral 1989, Universidad País Vasco, 294 pp. Servicio Editorial. ISBN 978-84-9860-178-7.
- Martín-González, F., Barbero, L., Capote, R., Heredia, N., & Gallastegui, G. (2012). Interaction of two successive Alpine deformation constraints from low-temperature thermochronology and structural mapping (NW Iberian Peninsula). *International Journal of Earth Sciences*, 101(5), 1331–1342. <https://doi.org/10.1007/s00531-011-0712-9>
- Masini, E., Manatschal, G., Tugend, J., Mohn, G., & Flament, J. M. (2014). The tectono-sedimentary evolution of a hyper-extended rift basin: The example of the Arzacq-Mauléon rift system (Western Pyrenees, SW France). *International Journal of Earth Sciences*, 103(6), 1569–1596. <https://doi.org/10.1007/s00531-014-1023-8>
- Mathy, B., Floquet, M., & Martínez-Torres, L. M. (1999). The Leiza palaeo-fault: Role and importance in the Upper Cretaceous sedimentation and palaeogeography of the Basque Pyrenees (Spain). *Comptes Rendus de l'Académie des Sciences - Series IIA - Earth and Planetary Science*, 328(6), 393–399. [https://doi.org/10.1016/S1251-8050\(99\)80105-0](https://doi.org/10.1016/S1251-8050(99)80105-0)
- Maurel, O., Monié, P., Pik, R., Arnaud, N., Brunel, M., & Jolivet, M. (2008). The Meso-Cenozoic thermo-tectonic evolution of the Eastern Pyrenees: An ⁴⁰Ar/³⁹Ar fission track and (U-Th)/He thermochronological study of the Canigou and Mont-Louis massifs. *International Journal of Earth Sciences*, 97(3), 565–584. <https://doi.org/10.1007/s00531-007-0179-x>
- Metcalfe, J. R., Fitzgerald, P. G., Baldwin, S. L., & Munoz, J. A. (2009). Thermochronology of a convergent orogen: Constraints on the timing of thrust faulting and subsequent exhumation of the Maladeta Pluton in the Central Pyrenean Axial Zone. *Earth and Planetary Science Letters*, 287(3-4), 488–503. <https://doi.org/10.1016/j.epsl.2009.08.036>

- Morris, R. G., Sinclair, H. D., & Yelland, A. J. (1998). Exhumation of the Pyrenean orogen: Implications for sediment discharge. *Basin Research*, 10, 69–85. <https://doi.org/10.1046/j.1365-2117.1998.00053.x>
- Mouthereau, F., Filleaudeau, P.-Y., Vacherat, A., Pik, R., Lacombe, O., Fellin, M. G., et al. (2014). Placing limits to shortening evolution in the Pyrenees: Role of margin architecture and implications for the Iberia/Europe convergence. *Tectonics*, 33, 2283–2314. <https://doi.org/10.1002/2014TC003663>
- Muñoz, J. A. (1992). Evolution of a continental collision belt: ECORS-Pyrenees crustal balanced cross-section. In K. R. McClay (Ed.), *Thrust Tectonics*. Dordrecht: Springer. <https://doi.org/10.1007/978-94-011-3066-021>
- Nirrengarten, M., Manatschal, G., Tugend, J., Kusznir, N., & Sauter, D. (2018). Kinematic Evolution of the Southern North Atlantic: Implications for the formation of hyperextended rift systems. *Tectonics*, 37, 89–118. <https://doi.org/10.1002/2017TC004495>
- Oliva-Urcia, B., Pueyo, E. L., Larrasoana, J. C., Casas, A. M., Román-Berdiel, T., van der Voo, R., & Scholger, R. (2012). New and revisited paleomagnetic data from Permian–Triassic red beds: Two kinematic domains in the west-central Pyrenees. *Tectonophysics*, 522–523, 158–175. <https://doi.org/10.1016/j.tecto.2011.11.023>
- Payros, A., Pujalte, V., & Orue-Etxebarria, X. (1999). The South Pyrenean Eocene carbonate megabreccias revisited: New interpretation based on evidence from the Pamplona Basin. *Sedimentary Geology*, 125(3–4), 165–194. [https://doi.org/10.1016/S0037-0738\(99\)00004-4](https://doi.org/10.1016/S0037-0738(99)00004-4)
- Payros, A., Pujalte, V., & Orue-Etxebarria, X. (2007). A point-sourced calciclastic submarine fan complex (Eocene Anotz Formation, western Pyrenees): Facies architecture, evolution and controlling factors. *Sedimentology*, 54, 137–168. <https://doi.org/10.1111/j.1365-3091.2006.00823.x>
- Pedreira, D., Afonso, J. C., Pulgar, J. A., Gallastegui, J., Carballo, A., Fernández, M., et al. (2015). Geophysical-petrological modeling of the lithosphere beneath the Cantabrian Mountains and the North-Iberian margin: Geodynamic implications. *Lithos*, 230, 46–68. <https://doi.org/10.1016/j.lithos.2015.04.018>
- Pedreira, D., Pulgar, J. A., Gallart, J., & Díaz, J. (2003). Seismic evidence of Alpine crustal thickening and wedging from the western Pyrenees to the Cantabrian Mountains (north Iberia). *Journal of Geophysical Research*, 108(B4), 2204. <https://doi.org/10.1029/2001JB001667>
- Pedreira, D., Pulgar, J. A., Gallart, J., & Torné, M. (2007). Three-dimensional gravity and magnetic modeling of crustal indentation and wedging in the western Pyrenees-Cantabrian Mountains. *Journal of Geophysical Research*, 112, B12405. <https://doi.org/10.1029/2007JB005021>
- Pérez-Arlucea, M., Carter, A., Clemente, F., González, D., & Nombela, M. (2005). Multi-approach, long and short term denudation rate calculations for the Galician Coast (Ría de Vigo, Spain): AFTD, DEM analysis, river loads and sediment budgets. *Journal of Coastal Research*, 9–14.
- Pik, R., Marty, B., Carignan, J., & Lavé, J. (2003). Stability of the Upper Nile drainage network (Ethiopia) deduced from (U-Th)/He thermochronometry: Implications for uplift and erosion of the Afar plume dome. *Earth and Planetary Science Letters*, 215(1–2), 73–88. [https://doi.org/10.1016/S0012-821X\(03\)00457-6](https://doi.org/10.1016/S0012-821X(03)00457-6)
- Poprawski, Y., Basile, C., Jaillard, E., Gaudin, M., & Lopez, M. (2016). Halokinetic sequences in carbonate systems: An example from the Middle Albian Bakio Breccias Formation (Basque Country, Spain). *Sedimentary Geology*, 334(1), 34–52. <https://doi.org/10.1016/j.sedgeo.2016.01.013>
- Pueyo Anchuela, O. (2004). Estructura y cinemática del Frente de Cabalgamiento Surpirenaico en el sector occidental de la Cuenca de Jaca-Pamplona, sierra de Alaiz. Universidad de Zaragoza.
- Pueyo Anchuela, O., Millán Garrido, H., Pocovi Juan, A., & Gil Imaz, A. (2007). Zona de transferencia en el sector occidental del Pirineo Central, ejemplo de la falla de Oroz-Betelu-Unzué. Zona Surpirenaica. Navarra. Geogaceta, 42, 19–22.
- Puigdefábregas, T., Rojas Tapia, B., Sánchez Carpintero, I., & Del Valle, J. (1976). Mapa Geológico de España E. 1:50.000. Hoja 142, Aoiz. Instituto Geológico y Minero de España, IGME.
- Pulgar, J. A., Gallart, J., Fernández-Viejo, G., Pérez-Estaún, A., Álvarez-Marrón, J., & ESCIN Group (1996). Seismic image of the Cantabrian Mountains in the western extension of the Pyrenees from integrated ESCIN reflection and refraction data. *Tectonophysics*, 264, 1–19.
- Quintana, L., Pulgar, J. A., & Alonso, J. L. (2015). Displacement transfer from borders to interior of a plate: A crustal transect of Iberia. *Tectonophysics*, 663, 378–398. <https://doi.org/10.1016/j.tecto.2015.08.046>
- Rahl, J. M., Haines, S. H., & van der Pluijm, B. A. (2011). Links between orogenic wedge deformation and erosional exhumation: Evidence from illite age analysis of fault rock and detrital thermochronology of syn-tectonic conglomerates in the Spanish Pyrenees. *Earth and Planetary Science Letters*, 307(1–2), 180–190. <https://doi.org/10.1016/j.epsl.2011.04.036>
- Ramírez Merino, J. J., Olivé Davo, A., Carballo Olivares, A., Villalobos Vilches, L., & León González, L. (1984). Mapa Geológico de España E. 1:50.000. Hoja 140, Estella. Instituto Geológico y Minero de España, IGME.
- Rat, J., Mouthereau, F., Bricchau, S., Crémades, A., Bernet, M., Balvay, M., et al. (2019). Tectonothermal evolution of the Cameros basin: Implications for tectonics of North Iberia. *Tectonics*, 38, 440–469. <https://doi.org/10.1029/2018TC005294>
- Rat, P. (1988). The Basque-Cantabrian basin between the Iberian and European plates some facts but still many problems. *Revista de la Sociedad Geológica de España*, 1, 3–4.
- Reiners, P. W. (2005). Zircon (U-Th)/He Thermochronometry. *Reviews in Mineralogy and Geochemistry*, 58(1), 151–179. <https://doi.org/10.2138/rmg.2005.58.6>
- Reiners, P. W., & Brandon, M. T. (2006). Using thermochronology to understand orogenic erosion. *Annual Review of Earth and Planetary Sciences*, 34(1), 419–466. <https://doi.org/10.1146/annurev.earth.34.031405.125202>
- Riba Arderiu, O. (1992). Las secuencias oblicuas en el borde Norte de la Depresión del Ebro en Navarra y la Discordancia de Barbarín. *Acta Geologica Hispánica*, 27(1–2), 55–68.
- Roca, E., Muñoz, J. A., Ferrer, O., & Ellouz, N. (2011). The role of the Bay of Biscay Mesozoic extensional structure in the configuration of the Pyrenean orogen: Constraints from the MARCONI deep seismic reflection survey. *Tectonics*, 30, TC2001. <https://doi.org/10.1029/2010TC002735>
- Rosenbaum, G., Lister, G. S., & Duboz, C. (2002). Relative motions of Africa, Iberia and Europe during Alpine orogeny. *Tectonophysics*, 359(1–2), 117–129. [https://doi.org/10.1016/S0040-1951\(02\)00442-0](https://doi.org/10.1016/S0040-1951(02)00442-0)
- Rosy, P., Cocherie, A., Fanning, C. M., & Ternier, Y. (2003). Datation U-Pb sur zircons des dolérites tholéïtiques pyrénéennes (ophites) à la limite Trias-Jurassique et relation avec les tufs volcaniques dits « infra-liasiques » nord-pyrénéens. C.R. *Geoscience*, 335(15), 1071–1080. <https://doi.org/10.1016/j.crte.2003.09.011>
- Ruiz, M., Díaz, J., Pedreira, D., Gallart, J., & Pulgar, J. A. (2017). Crustal structure of the North Iberian continental margin from seismic refraction/wide-angle reflection profiles. *Tectonophysics*, 717, 65–82. <https://doi.org/10.1016/j.tecto.2017.07.008>
- Ruiz, M., Gallart, J., Díaz, J., Olivera, C., Pedreira, D., López, C., et al. (2006). Seismic activity at the western Pyrenean edge. *Tectonophysics*, 412(3–4), 217–235. <https://doi.org/10.1016/j.tecto.2005.10.034>

- Ruiz, M., Gaspà, O., Gallart, J., Díaz, J., Pulgar, J. A., García-Sansegundo, J., et al. (2006). Aftershocks series monitoring of the September 18, 2004 M=4.6 earthquake at the western Pyrenees: A case of reservoir-triggered seismicity? *Tectonophysics*, 424, 223–243. <https://doi.org/10.1016/j.tecto.2006.03.037>
- Rushlow, C. R., Barnes, J. B., Ehlers, T. A., & Vergés, J. (2013). Exhumation of the southern Pyrenean fold-thrust belt (Spain) from orogenic growth to decay. *Tectonics*, 32, 843–860. <https://doi.org/10.1002/tect.20030>
- Saspiturry, N., Razin, P., Baudin, T., Serrano, O., Issautier, B., Lasseur, E., et al. (2019). Symmetry vs. asymmetry of a hyper-thinned rift: Example of the Mauléon Basin (Western Pyrenees, France). *Marine and Petroleum Geology*, 104, 86–105. <https://doi.org/10.1016/j.marpetgeo.2019.03.031>
- Schott, J. J., & Peres, A. (1988). Paleomagnetism of Permo-Triassic red beds in the western Pyrenees: Evidence for strong clockwise rotations of the Paleozoic units. *Tectonophysics*, 156(1–2), 75–88. [https://doi.org/10.1016/0040-1951\(88\)90284-3](https://doi.org/10.1016/0040-1951(88)90284-3)
- Sibuet, J.-C., Srivastava, S. P., & Spakman, W. (2004). Pyrenean orogeny and plate kinematics. *Journal of Geophysical Research*, 109, B08104. <https://doi.org/10.1029/2003JB002514>
- Sinclair, H. D., Gibson, M., Naylor, M., & Morris, R. G. (2005). Asymmetric growth of the Pyrenees revealed through measurement and modeling of orogenic fluxes. *American Journal of Science*, 305(5), 369–406. <https://doi.org/10.2475/ajs.305.5.369>
- Teixell, A. (1996). The Ansó transect of the southern Pyrenees: Basement and cover thrust geometries. *Journal of the Geological Society*, 153(2), 301–310. <https://doi.org/10.1144/gsjgs.153.2.0301>
- Teixell, A. (1998). Crustal structure and orogenic material budget in the west central Pyrenees. *Tectonics*, 17(3), 395–406. <https://doi.org/10.1029/98TC00561>
- Teixell, A., & García-Sansegundo, J. (1995). Estructura del sector central de la Cuenca de Jaca (Pirineos meridionales). *Revista de la Sociedad Geológica de España*, 8(3), 215–228.
- Teixell, A., Labaume, P., Ayarza, P., Espurt, N., De Saint Blanquat, M., & Lagabriele, Y. (2018). Crustal structure and evolution of the Pyrenean-Cantabrian belt: A review and new interpretations from recent concepts and data. *Tectonophysics*, 724–725, 146–170. <https://doi.org/10.1016/j.tecto.2018.01.009>
- Teixell, A., Labaume, P., & Lagabriele, Y. (2016). The crustal evolution of the west-central Pyrenees revisited: Inferences from a new kinematic scenario. *Comptes Rendus Geoscience*, 348(3–4), 257–267. <https://doi.org/10.1016/j.crte.2015.10.010>
- Tibari, B., Vacherat, A., Stab, M., Pik, R., Yeghicheyan, D., & Hild, P. (2016). An alternative protocol for single zircon dissolution with application to (U-Th-Sm)/He Thermochronometry. *Geostandards and Geolanalytical Research*, 40(3), 365–375. <https://doi.org/10.1111/j.1751-908X.2016.00375.x>
- Tilhac, R., Guillaume, D., & Odonne, F. (2013). Fluid circulation and deformational gradient in north-Pyrenean flyschs: Example from the Saint-Jean-de-Luz basin (France). *Tectonophysics*, 608, 832–846. <https://doi.org/10.1016/j.tecto.2013.07.035>
- Tugend, J., Manatschal, G., & Kusznir, N. J. (2015). Spatial and temporal evolution of hyperextended rift systems: Implication for the nature, kinematics, and timing of the Iberian-European plate boundary. *Geology*, 43(1), 15–18. <https://doi.org/10.1130/G36072.1>
- Tugend, J., Manatschal, G., Kusznir, N. J., Masini, E., Mohn, G., & Thion, I. (2014). Formation and deformation of hyperextended rift systems: Insights from rift domain mapping in the Bay of Biscay Pyrenees. *Tectonics*, 33, 1239–1276. <https://doi.org/10.1002/2014TC003529>
- Vacherat, A., Mouthereau, F., Pik, R., Bellahsen, N., Gautheron, C., Bernet, M., et al. (2016). Rift-to-collision transition recorded by tectono-thermal evolution of the northern Pyrenees. *Tectonics*, 35, 907–933. <https://doi.org/10.1002/2015TC004016>
- Vacherat, A., Mouthereau, F., Pik, R., Bernet, M., Gautheron, C., Masini, E., et al. (2014). Thermal imprint of rift-related processes in orogens as recorded in the Pyrenees. *Earth and Planetary Science Letters*, 408, 296–306. <https://doi.org/10.1016/j.epsl.2014.10.014>
- Vacherat, A., Mouthereau, F., Pik, R., Huyghe, D., Paquette, J.-L., Christophoul, F., et al. (2017). Rift-to-collision sediment routing in the Pyrenees: A synthesis from sedimentological, geochronological and kinematic constraints. *Earth-Science Reviews*, 172, 43–74. <https://doi.org/10.1016/j.earscirev.2017.07.004>
- van der Voo, R. (1969). Paleomagnetic evidence for the rotation of the Iberian Peninsula. *Tectonophysics*, 7, 5–56. [https://doi.org/10.1016/0040-1951\(69\)90063-8](https://doi.org/10.1016/0040-1951(69)90063-8)
- van der Voo, R., & Boessenkool, A. (1973). Permian paleomagnetic results from the western Pyrenees; delineating the plate boundary between the Iberian Peninsula and stable Europe. *Journal of Geophysical Research*, 78(23), 5118–5127.
- van Hinsbergen, D. J. J., Spakman, W., Vissers, R. L. M., & van der Meer, D. G. (2017). Comment on “Assessing discrepancies between previous plate kinematic models of Mesozoic Iberia and their constraints” by Barnett-Moore et al. *Tectonics*, 36, 3277–3285. <https://doi.org/10.1002/2016TC004418>
- Velasco, F., Pesquera, A., Arce, R., & Olmedo, F. (1987). A contribution to the ore genesis of the magnesite deposit of Eugui, Navarra (Spain). *Mineralium Deposita*, 22(1), 33–41.
- Vergés, J., Fernández, M., & Martínez, A. (2002). The Pyrenean orogen: Pre-, syn-, and post-collisional evolution. In G. Rosenbaum & G. Lister (Eds.), *Reconstruction of the evolution of the Alpine-Himalayan Orogen*. *Journal of Virtual Explorer*, 8(4), 55–74. <https://doi.org/10.3809/jvirtex.2002.00058>
- Vergés, J., Millan, H., Roca, E., Muñoz, J. A., Marzo, M., Cirés, J., et al. (1995). Eastern Pyrenees and related foreland basins: Pre-, syn- and post-collisional crustal-scale cross-sections. *Marine and Petroleum Geology*, 12(8), 893–915.
- Vermeesch, P. (2018). IsoplotR: A free and open toolbox for geochronology. *Geoscience Frontiers*, 9(5), 1479–1493. <https://doi.org/10.1016/j.gsf.2018.04.001>
- Vermeesch, P., & Tian, Y. (2014). Thermal history modelling: HeFTy vs. QTQt. *Earth Science Reviews*, 139, 279–290. <https://doi.org/10.1016/j.earscirev.2014.09.010>
- Vermeesch, P., & Tian, Y. (2018). Reply to Comment on “Thermal history modelling: HeFTy vs. QTQt” by K. Gallagher and R.A. Ketcham. *Earth-Science Reviews*, 176, 395–396. <https://doi.org/10.1016/j.earscirev.2017.11.015>
- Wagner, G. A., & van der Haute, P. (1992). Fission-Track dating. Ferdinand Enke Verlag Stuttgart, DOI: <https://doi.org/10.1007/978-94-011-2478-2>.
- Whitchurch, A. L., Carter, A., Sinclair, H. D., Duller, R. A., Whittaker, A. C., & Allen, P. A. (2011). Sediment routing system evolution within a diachronously uplifting orogen: Insights from detrital zircon thermochronological analyses from the South-Central Pyrenees. *American Journal of Science*, 311(5), 442–482. <https://doi.org/10.2475/05.2011.03>
- Yelland, A. J. (1990). Fission track thermotectonics in the Pyrenean orogen. *International Journal of Radiation Applications and Instrumentation. Part D. Nuclear Tracks and Radiation Measurements*, 17(3), 293–299. [https://doi.org/10.1016/1359-0189\(90\)90049-4](https://doi.org/10.1016/1359-0189(90)90049-4)
- Ziegler, P. A. (1989). Evolution of the North Atlantic: An overview. In A. J. Tankard & H. R. Balkwill (Eds.), *Extensional tectonics and stratigraphy of the North Atlantic margins*, AAPG Mem. 46.